RIV000127
Submitted: October 11, 2012

The Point Defect Model for the Passive State

Digby D. Macdonald*

Center for Advanced Materials, The Pennsylvania State University, University Park, Pennsylvania 16802

ABSTRACT

A review is presented of the point defect model (PDM) for the growth and breakdown of passive films on metal and alloy surfaces in contact with aqueous solutions. The model provides a reasonable account of the steady-state properties of cation-conducting and anion-conducting barrier layers on nickel and tungsten, respectively, in phosphate buffer solutions; of the impedance characteristics of passive films on nickel; of the breakdown of passive films on a wide range of metals and alloys; of the distributions in the breakdown parameters (breakdown voltage and induction time); of the role of alloying elements in enhancing the resistance of alloys to passivity breakdown; of transpassive dissolution and electropolishing; of erosion-corrosion; and of photoinhibition of pit nucleation. Additionally, the PDM has allowed us to formulate a set of principles for designing new alloys and has led to the development of a deterministic method for predicting localized corrosion damage functions.

The passivity of metals and alloys is the single most important phenomenon responsible for our metals-based civilization. We all accept metals technology in our everyday lives, but few of us realize that most structural metals are viable in an engineering sense only because of the existence of a surface oxide film whose thickness may not exceed a few nanometers (several tens of atomic diameters). These films frequently isolate phases that, without kinetic restrictions, ordinarily react violently. Consider, for example, one of our most common structural metals, aluminum. This metal has a heat and a free energy of reaction with oxygen that are not too different from those for gasoline, yet everday we fly through the air in vehicles made from the former but powered by the latter. The continued structural integrity of the aircraft is due entirely to the aluminum oxide film that exists on the surface. Extensive rupture of this film over large areas of the surface can lead to catastrophic reaction of the underlying metal with the environment. For example, powdered aluminum is added to solid rocket fuels to boost the energy density of the propellant. Likewise, the aluminum superstructure of the frigate HMS Sheffield burned during the Falkland-Malvinas Island war after being struck by an anti-ship missile. In both cases, factors existed that rendered the oxide film on the surface mechanically and structrually unstable, resulting in the continued exposure of the underlying metal to oxygen at highly elevated temperatures.

Electrochemists are familiar with passivity, because it leads to the sudden drop in the current flowing across a metal/solution interface on anodic polarization, when the potential exceeds a critical value (Fig. 1). At potentials more negative than this value, the metal dissolves in the active state where the surface is more-or-less uncovered by an oxidation product film.[a] At some critical potential, a transition occurs at the surface resulting in the formation of a phase, possibly of monoatomic dimensions, that effectively isolates the metal from the environment. A number of mechanisms could be responsible for this transition, including the chemisorption of oxygen at the interface, the coalescence of oxide islands on the surface to form a continuous film, or perhaps the dehydration (possibly induced by deprotonation) of a thin oxyhydroxide precursor. Regardless of the exact mechanism of this process, the transition is remarkable in that the current may drop by many orders in magnitude when the potential is increased in the positive direction by no more than a few millivolts.

Here I review the development of the PDM for the growth and breakdown of passive films on metal surfaces.[2-13] Carl Wagner made significant contributions to this subject. Similarities between Wagner's theory of (dry) oxidation[14] and the PDM for anodic films are discussed; both theory and model assume that the principal entities involved in oxide growth are point defects, notably cation (V_M'') and anion ($V_O^{\cdot\cdot}$) vacancies, in a disordered barrier layer of nominal stoichiometry $MO_{\chi/2}$.

Steady-state Passive Films

Although the phenomenon of passivity has been known for more than 150 years, during which time numerous theories have been proposed to explain the effect,[14-19] a satisfactory description of the passive state still eludes us. This state of affairs is due, in part, to the experimental difficulties in probing surface films whose thickness may not exceed a few nanometers, and also is due to the conceptual difficulty in using bulk phase concepts in formulating theoretical descriptions. Any theory must explain some well-established experimental facts, including:

1. Passive films generally form as bilayers, with a highly disordered "barrier" layer adjacent to the metal and an outer film comprised of a precipated phase that may incorporate anions and/or cations from the solution (Fig. 2). Because passivity still is observed in the absence of the outer film (*e.g.*, in highly acidic or basic solutions where precipitation may not occur), we attribute "passivity" to the barrier layer.
2. The steady-state thickness of the barrier layer and logarithm of the steady-state current generally vary lin-

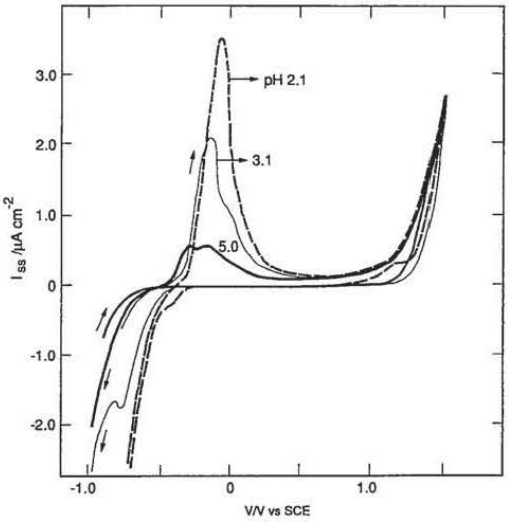

Fig. 1. Potentiodynamic curves for a single-crystal Ni(100) electrode in phosphate buffer solutions at various pH values (indicated on the curves). Sweep rate = 20 mV s^{-1}; electrode area, A = 1.25 cm^2.

* Electrochemical Society Active Member.

[a] It is not at all certain that the surface in the active state is "bare". For example, Wright[1] found that iron in sulfuric acid, in the active state, exhibits an anodic photocurrent. The only viable explanation of this effect is that the surface is covered by a film whose properties and thickness are such that electronic transition can occur resulting in the generation of mobile charge.

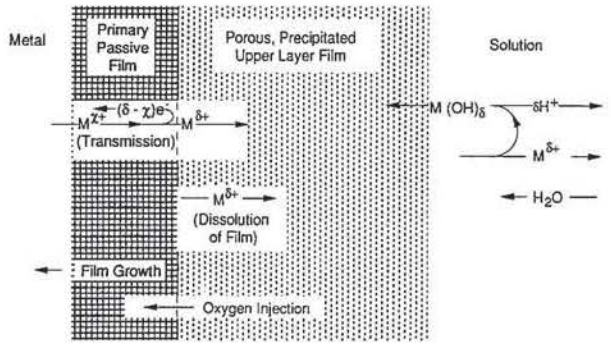

Fig. 2. Schematic of processes that lead to the formation of bilayer passive films on metal surfaces.

early with the applied voltage, except when a change in oxidation state of the cation within the film occurs within the passive range. The linear variation of the film thickness with applied voltage implies that the electric space field within the film is also independent of voltage, even under controlled potential conditions. This hypothesis is contrary to the potential-dependent field assumed in previous treatments.

3. Marker experiments,[20] and the segregation of alloying elements into the barrier layer, as determined by using surface analysis by laser ionization (SALI), are consistent with the growth of the barrier layer into the metal phase. Likewise, marker studies, and structural and compositional factors are consistent with the upper layer growing outwards from the barrier layer/environment interface.

Perhaps the simplest case to treat from an analytical viewpoint is that of a film under steady-state conditions. We have developed this case recently for the two extreme kinetic behaviors of interfacial equilibrium and irreversible reaction.[5,6] Only the latter case will be described in any detail here, but the diagnostic criteria derived from the interfacial equilibrium model are included for completeness.

Assuming that the transmission of ions through the barrier layer occurs by vacancy motion, due to the preponderance of Schottky defects, the reactions that occur at the metal/film and film/solution interfaces are those depicted in Fig. 3. The reactions shown are not assumed; they are the only possible elementary reactions for vacancy generation and annihilation. The reactions given in Fig. 3 differ fundamentally in terms of whether they conserve the film boundary with respect to some fixed reference point in space. Reactions 1, 3, and 4 conserve the film, because they involve the movement of ions across the boundaries. Reaction 2 results in the generation of new film [$M_M + (\chi/2)\ V_{\ddot{O}}$] by a fluctuation in electron density around an atom in the metal at the metal/film boundary. The metal atom (m) does not move substantially, but some movement of the ions within the film must occur to create the oxygen vacancy.[b] Likewise, reaction 5 results in the destruction of the film by dissolution (which may or may not be an electrochemical process), and hence, is also nonconservative.

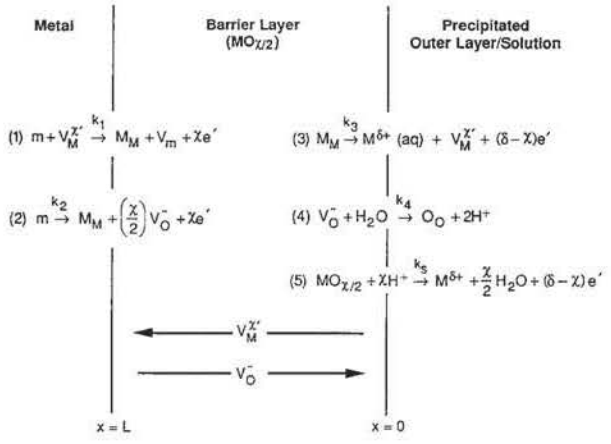

Fig. 3. Schematic of physicochemical processes that occur within a passive film according to the point defect model. m = metal atom, M_M = metal cation in cation site, O_O = oxygen ion in anion site, $V_M^{\chi'}$ = cation vacancy, $V_{\ddot{O}}$ = anion vacancy, V_m = vacancy in metal phase. During film growth, cation vacancies are produced at the film/solution interface, but are consumed at the metal/film interface. Likewise, anion vacancies are formed at the metal/film interface, but are consumed at the film/solution interface. Consequently, the fluxes of cation vacancies and anion vacancies are in the directions indicated. Note that reaction 1, 3, and 4 are lattice conservative processes, whereas reaction 2 and 5 are not.

Because the steady-state must involve two nonconservative reactions (only one nonconservative reaction would result in monotonic growth or thinning of the film), the rates of reactions 2 and 5 must be equal, resulting in

$$\left[[J_o]_{m/f} = -\left(\frac{\chi}{2}\right) k_s C_{H^+}^n\right]_{f/s} \quad [1]$$

where J_o is the flux of oxygen vacancies at the metal/film interface, χ is the barrier layer stoichiometry ($MO_{\chi/2}$), k_s is the (potential-dependent) rate constant for the dissolution of the barrier layer, and n is the kinetic order of this process with respect to protons.[5-6] Similarly, we may express the total current flowing into the metal as

$$I_{SS} = F[\delta J_M - 2J_o + (\delta - \chi)k_s C_{H^+}^n] \quad [2]$$

where J_M is the flux of cation vacancies from the film/solution interface to the metal/film interface. Substitution of Eq. 1 yields a somewhat simpler expression as

$$I_{ss} = \delta F[J_M + k_s C_{H^+}^n] \quad [3]$$

Equation 3 is important, because it demonstrates that, in the steady-state, the current is determined by the flux of cation vacancies and by the kinetics of film dissolution (which is related to J_o through Eq. 1). Of course, this expression is strictly valid only in the absence of redox species in the environment, which would result in parallel electron or hole currents of magnitudes that depend on the thickness of the film (among other factors).

By expressing the interfacial rate constants as exponential functions of the interfacial potential differences, and by assuming that the potential drop across the film/solution interface, $\phi_{f/s}$, varies linearly with applied voltage (Fig. 4) and pH

$$\phi_{f/s} = \alpha V + \beta pH + \phi_{f/s}^o \quad [4]$$

we have been able to derive expressions for the steady-state thickness of the barrier layer and the steady-state current as[5,6]

$$L_{ss} = \frac{1}{\varepsilon}\left[1 - \alpha - \frac{\alpha\alpha_d}{\alpha_2}\left(\frac{\delta}{\chi} - 1\right)\right] V + \frac{1}{\varepsilon}\left\{\frac{2.303n}{\alpha_2\chi\gamma} - \beta\left[\frac{\alpha_d}{\alpha_2}\left(\frac{\delta}{\chi} - 1\right) + 1\right]\right\} pH + \frac{1}{\alpha_2\chi K}\ln\left(\frac{k_2^o}{k_s^o}\right) \quad [5]$$

and

$$I_{ss} = \delta F[k_3^o e^{\alpha_3\alpha\gamma V} e^{\alpha_3\beta\gamma pH} + k_s^o e^{\alpha_d\alpha(\delta-\chi)\gamma V} e^{\beta\alpha_d(\delta-\chi)\gamma pH} C_{H^+}^n] \quad [6]$$

where k_i^o and α_i are the standard rate constant and transfer coefficient for the i-th reaction (Fig. 3), $\gamma = F/RT$, and α_d is the transfer coefficient for the film dissolution reaction. Equation 5 successfully accounts for the observed linear dependence of L_{ss} on V.[c] Likewise, L_{ss} is predicted to vary linearly with pH and this relationship also is found for many systems (Fig. 5). Finally, provided that either cation vacancies or anion vacancies dominate the transport properties of the barrier layer, Eq. 6 predicts that the logarithm of the steady-state current will vary linearly with applied voltage, as is also commonly found experimentally.

[b] Or, perhaps, cation vacancies are converted to anion vacancies?

[c] L_{SS} varies linearly with V for many systems; this relationship is so reliable that, in the case of the valve metals, the thickness of anodic films frequently is expressed in terms of the anodizing voltage.

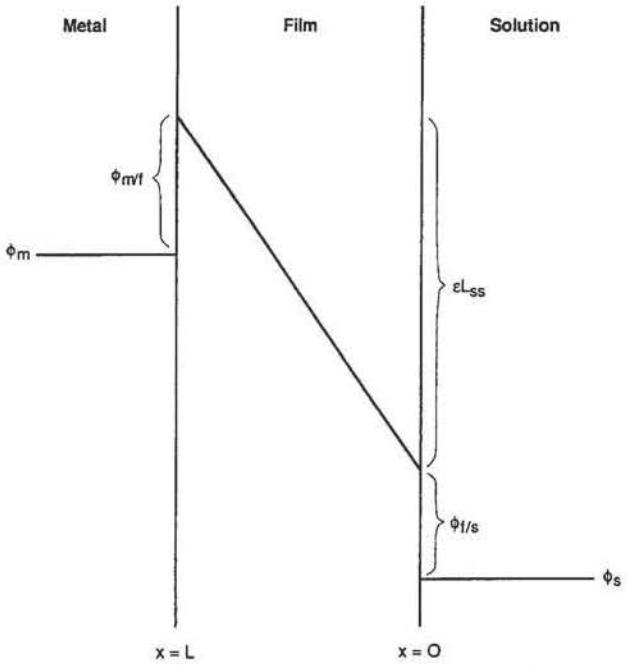

Fig. 4. Schematic potential profile across a passive film.

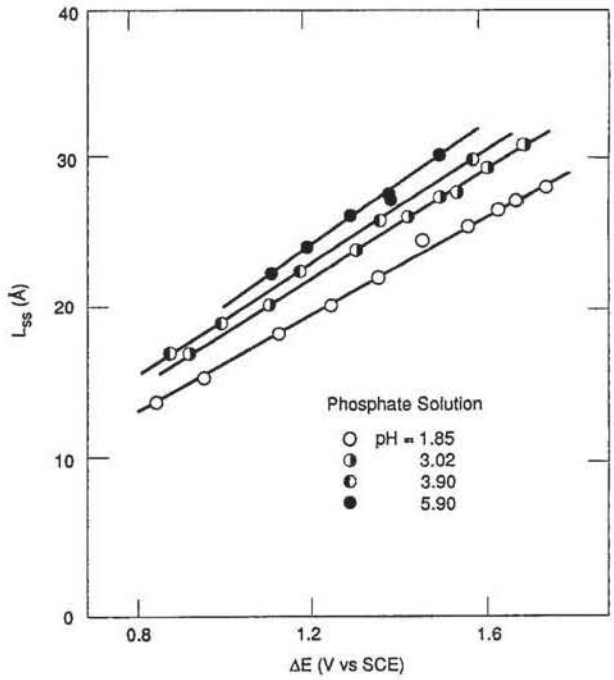

Fig. 5. Thickness of the barrier oxide layer on iron in acidic phosphate solutions as a function growth potential (after Sato and Noda, Ref. 19).

The predicted dependencies of L_{ss} and $\ln(I_{ss})$ on the applied voltage, pH, and cation concentration in solution (including those for the interfacial equilibrium case) give rise to the diagnostic criteria listed in Table I, which may be used to identify the majority (vacancy) charge carrier in the film and to characterize the kinetic natures of the interfacial reactions. Recently we have applied these criteria to characterize the passive films on nickel and tungsten; two systems that are thought to represent the extremes in passive film behavior, because of the large difference in oxidation states of the cations (Ni^{2+} *vs.* W^{6+}). In carrying out this analysis, we chose to use (partly for experimental convenience) the steady-state current as the experimentally dependent variable and applied voltage, pH, and dissolution product concentration as the independent variables.

The diagnostic functions summarized in Table I have been employed recently to explore the nature of the passive film on single crystal nickel (100) in phosphate buffer solution.[6] In agreement with theory, log (I_{ss}) varies linearly with applied voltage (excluding deviations close to the active-to passive transition for the three most acidic solutions), with a slope that is independent of pH. Likewise, and again in agreement with theory (for a constant value for n), log (I_{ss}) varies linearly with pH and the steady-state current is found to be independent of $[Ni^{2+}]$ over a wide range of concentration. Noting that $\delta = \chi$, for this case, these data are consistent only with the passive film on nickel being a cation conductor involving irreversible ejection of cations from the film.

In the case of tungsten[6] in the same phosphate medium, the steady-state current is independent of both the applied voltage and tungstate concentration. Because, in this case as well, $\delta = \chi$, the data are consistent with the passive film on tungsten being an anion (oxygen ion) conductor under either interfacial equilibrium or kinetic control. In both cases, the gradients of log (I_{ss}) *vs.* pH should be equal to $-n$, where n is the kinetic order of the barrier layer dissolution reaction with respect to hydrogen ion in solution. Although considerable scatter exist in the data,[6] this prediction holds with $n = 1$ and -1 at low and high pH values, respectively, corresponding to the dissolution of the WO_3 barrier layer presumably as

$$WO_3 + 2H^+ \rightarrow WO_2^{2+} + H_2O \qquad [7]$$

Table I. Diagnostic criteria for determining the conductive nature of the barrier layer.

	Interfacial equilibrium		Kinetic control	
Criterion	Cation transmission	Anion transmission	Cation transmission	Anion transmission
$\left(\frac{\partial L_{ss}}{\partial V}\right)_{pH\ C_{M^{n+}}}$	$\left[1-\alpha-\frac{\alpha\alpha_d(\delta-\chi)}{2}\right]/\varepsilon$		$\left[1-\alpha-\frac{\alpha\alpha_d}{\alpha_2}\left(\frac{\delta}{\chi}-1\right)\right]/\varepsilon$	
$\left[\frac{\partial L_{ss}}{\partial pH}\right]_{V\ C_{M^{n+}}}$	$\left[\frac{1.1515n}{\gamma}-\beta\right]/\varepsilon$		$\left[\frac{2.303n}{\alpha_2\chi\gamma}-\beta\left(\frac{\alpha_d(\delta-\chi)}{\alpha_2\chi}\right)+1\right]/\varepsilon$	
$\left(\frac{\partial L_{ss}}{\partial \ln C_{M^{n+}}}\right)_{V\ pH}$	0		0	
$\left[\frac{\partial \ln (I_{ss})}{\partial V}\right]_{pH\ C_{M^{n+}}}$	$\delta\alpha\gamma$	$\alpha\alpha_d(\delta-\chi)\gamma$	$\alpha_3\alpha\gamma$	$\alpha\alpha_d(\delta-\chi)\gamma$
$\left[\frac{\partial \ln (I_{ss})}{\partial pH}\right]_{V\ C_{M^{n+}}}$	$\delta\beta\gamma$	$-2.303n$	$\alpha_3\beta\gamma$	$\beta\alpha_d(\delta-\chi)\gamma-2.303n$
$\left[\frac{\partial \ln (I_{ss})}{\partial \ln C_{M^{n+}}}\right]_{V\ pH}$	-1	0	0	0

(although the WO_2^{3+} species apparently has not been reported previously) in the more acidic solutions, and as

$$WO_3 + H_2O \rightarrow WO_4^{2-} + 2H^+ \quad [8]$$

in the less acidic solutions. The values of n indicate that reactions 7 and 8 are first order in H^+ and OH^-, respectively. Furthermore, the $\log(I_{ss})$ *vs.* pH correlations should intersect at a pH value given by

$$pH = \Delta G^\circ / 9.212\, RT \quad [9]$$

where ΔG° is the change in standard Gibbs energy for the equilibrium

$$WO_2^{2+} + 2H_2O \rightleftarrows WO_4^{2-} + 4H^+ \quad [10]$$

Using thermodynamic data for WO_4^{2-} given by Naumov *et al.*,[21] Eq. 9 yields a standard Gibbs energy of formation for WO_2^{2+} of −122.9 kcal/mol. Notwithstanding the uncertainty in the existence of WO_2^{2+}, the PDM clearly provides a quantitative account of the properties of steady-state passive films on nickel and tungsten, at least as can be probed using the passive current.

Now I return to the linear dependence of L_{ss} on applied voltage as found experimentally for many systems (Fig. 5) and as predicted by Eq. 5. No assumption was made in developing the PDM as to any functional dependence of ε on V. That L_{ss} varies linearly with voltage is powerful evidence that the electric field strength is independent of the applied voltage, even under controlled potential conditions. The alternative explanation is that the potential dependencies of ε and the quantity in square brackets in the first term on the right-hand side of Eq. 5 are exactly complementary, such that their product is independent of V over a wide range of voltage (*i.e.*, across the passive range). We consider this possibility remote.

The Impedance Characteristics of Passive Films

While the PDM successfully accounts for many properties of steady-state passive films, as discussed above, and provides powerful diagnostic criteria for classifying films according to the identity of the (vacancy) charge carrier and kinetic natures of the interfacial reactions, a much more severe test of the model's veracity is its ability to account for the impedance function over wide ranges of frequency and voltage. This is the "ultimate" test of the electrochemical predictions of the model, because the impedance function, when measured over an infinite frequency bandwidth, contains all the information that can be gleaned from a linear system by electrical means. Other (nonelectrical) experimental techniques provide additional information and nonlinear electrical methods (*e.g.*, harmonic impedance spectroscopy) provide still more. Nevertheless, EIS (electrochemical impedance spectroscopy) is a powerful diagnostic technique that is finding extensive use in mechanistic electrochemistry.

Starting with the work of Chao, Lin, and Macdonald[4] in 1982, we have used EIS to explore the properties of passive films that form on nickel in both phosphate and borate buffer solutions.[6-8] The most complete study of this kind was published recently by Macdonald and Smedley,[7,8] which explored the passive film on Ni(III) in phosphate buffer solutions over a wide frequency range (10 kHz – 1 MHz) and as a function of applied potential and pH. The version of the PDM used to fit the experimental data (using a nonlinear minimization procedure) is identical to that shown in Fig. 3, except that dissolution of the barrier layer was ignored in the impedance analysis. However, the linear dependence of L_{ss} on V was incorporated, so that the concept of the steady-state being dictated by the balance between two nonconservative processes is preserved.

The nonlinear minimization procedure uses a "design optimization" algorithm to minimize the object function

$$P = \sum_{i=1}^{n} \frac{\ln|Z_{exp}|_i - \ln|Z_{calc}|_i}{\ln|Z_{calc}|_i} \quad [11]$$

subject to the constraint

$$\sum_{i=1}^{n} \frac{[\sigma_{exp,i} - \sigma_{calc,i}]}{\sigma_{calc,i}} < 0.1 \quad [12]$$

where $|Z|$ is the impedance modulus, ϕ is the phase angle, and subscripts "exp" and "calc" are the experimentally-measured and calculated (from the PDM) quantities, respectively.

Fits of the PDM to the experimental impedance data were carried out by regarding various model parameters as variables. These parameters included the interfacial rate constants and transfer coefficients, electric field strength, and vacancy diffusivities (not all were varied simultaneously). It was necessary to assume a potential-dependent capacitance in parallel with the interfacial impedance to obtain a good simulation of the experimental data. A comparison between the optimum calculated impedance data and the experimental data for applied voltages of 0.1 and 0.5 V (SCE) and for a pH value of 9 is shown in Fig. 6. The calculated data were derived assuming that cation vacancies alone move through the barrier layer and a single set of kinetic parameters yielded a calculated impedance function that is in excellent agreement with the experimental data over wide ranges of voltage (0.1-0.5 V *vs.* SCE) and pH. However, the full set of simulations were carried out[7,8] for the two cases where we assume that either cation vacancies or oxygen vacancies within the barrier layer are mobile. Analysis of the two cases (cation *vs.* anion motion) found that the fits to the cation conducting case were significantly better than for the oxygen ion conducting case. This finding is consistent with our steady-state work discussed in the previous section (although that work was carried out at a later date), from which we also concluded that the barrier layer on nickel is a cation conductor. Furthermore, the optimization required the electric field to be independent of applied voltage, again in good agrement with the steady-state work. Interestingly, the fit was quite insensitive to values chosen for the kinetic parameters for the reactions occurring at the film/solution interface; we believe that this is because the system was not probed at a sufficiently low frequency (*i.e.*, sufficiently close to the steady-state) that processes occurring at the film/solution interface could be detected. Furthermore, the transfer coefficients found for the forward and reverse directions of reaction 1 in Fig. 3 were very small (~0.003), indicating extraordinarily low dependencies of the interfacial reaction (injection of cations into the film) on the local potential difference across the metal/film interface.

The steady-state work and the EIS studies provide a consistent story—the barrier layer on nickel in phosphate buffer solutions is a cation conductor that, under anodic polarization conditions, involves the irreversible ejection of cations from the film. However, in the steady-state work, we have described but two extremes in behavior; the case where all interfacial reactions are either in equilibrium or are completely irreversible. Presumably, a spectrum of intermediate cases exists where each of the interfacial reactions exhibits varying degrees of reversibility, and these cases need to be explored. Finally, we have completed extensive EIS studies recently on tungsten in phosphate buffer solution and the impedance spectra are substantially different from those for nickel in the same environments. According to our steady-state work, the passive film on tungsten is an oxygen ion conductor and the passive current presumably is dominated by the kinetics of dissolution of the barrier layer. These data currently are being analyzed in terms of the PDM by incorporating film dissolution (reaction 5, Fig. 3) and the findings will be published later. The PDM has successfully met every test to date, however only a few of the important properties of passive films have been probed. The argument for the basic validity of the PDM would be considerably stronger if the full complement of the diagnostic criteria summarized in Table I, along with the diagnostic features of EIS, could be applied to systems spanning the spectrum of kinetic behaviors de-

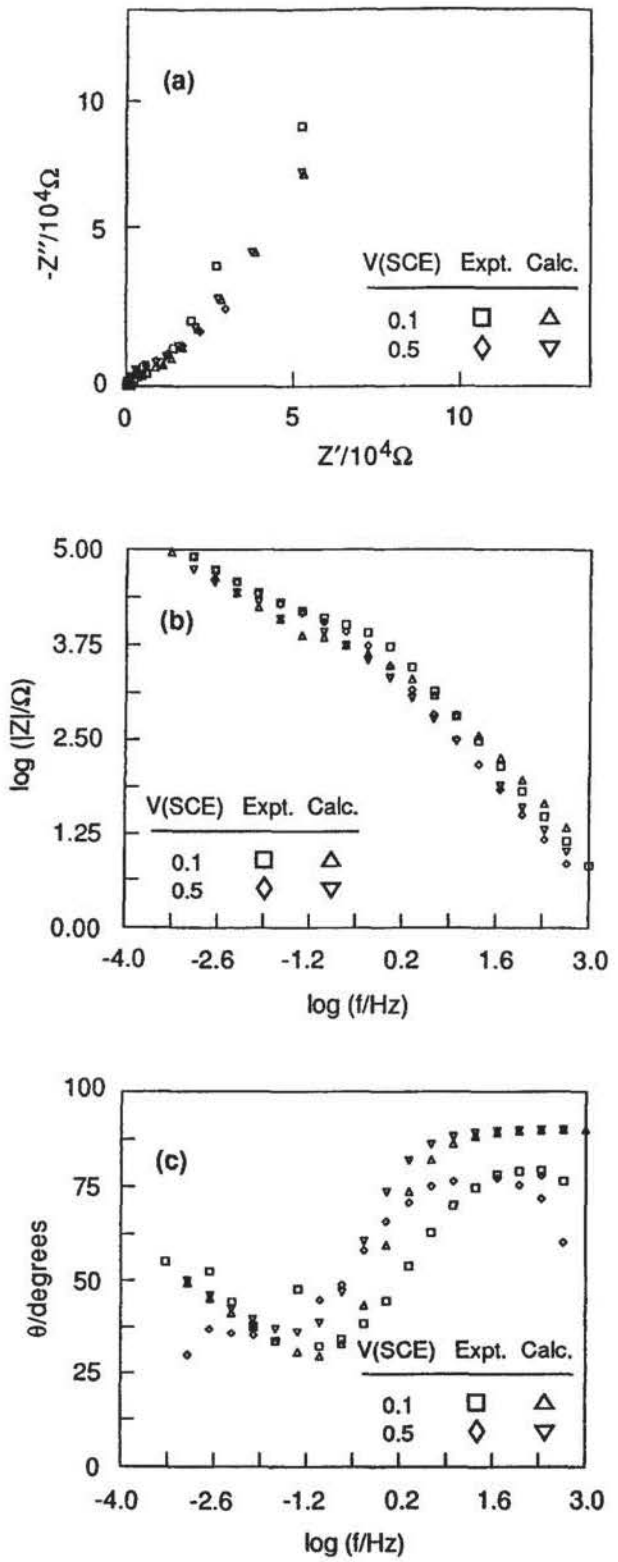

Fig. 6. Experimental and calculated impedance data for Ni(III) in 0.1*N* H_3PO_4/NaOH buffer solution, pH = 9, at 23 ± 2°C assuming that cation vacancies alone are mobile in the barrier film; (a, top) $-Z''$ *vs.* Z', (b, middle) log $|Z|$ *vs.* log f, (c, bottom) ϕ *vs.* log (f).

scribed above. This paper presents but one small step in this task.

Passivity Breakdown and Pit Nucleation

If the passive films on metals, such as those on iron, nickel, and chromium (and alloys thereof), remained completely intact then the corrosion current flowing across the interface under most industrial conditions would be of the order of 0.1-1.0 μA/cm², corresponding to corrosion rates of approximately 1.5×10^{-4} to 1.5×10^{-3} cm/yr (*i.e.*, 1.5 to 15 μm/yr). For most practical situations, metal loss rates of this order are of no concern so that our automobiles, bridges, airplanes, and industrial systems would last for times extending well beyond the current design lifetimes. Unfortunately, passive films do not remain intact, as we indicated in the case of aluminum at the beginning of this paper. Passivity breakdown can occur for various reasons, including straining of the substrate metal, the presence of thermal stresses (due to differences in thermal expansivity), fluid flow and cavitation, transpassivity polarization, and chemically induced phenomena. In the following discussion, we deal with three reasons for passivity breakdown. The three, pitting corrosion, transpassive dissolution, and erosion-corrosion are responsible for losses of many billions of dollars per annum to the US economy.

Pitting corrosion.—The best known causative agent of "chemically induced breakdown" is chloride ion, which shows a remarkable ability to cause pitting on many metals and alloys of industrial interest.[15-17] Assuming that an ion, like chloride, must interact physically with the barrier layer to cause passivity breakdown, and hence to nucleate pits, we ourselves explore how this might happen on an atomistic scale. Let us envision a hydrated chloride ion ($Cl^- \cdot nH_2O$, $n \approx 6$) approaching the film/solution interface of the barrier layer (after moving through the precipitated layer). From this vantage point, the barrier layer appears as an undulating surface of charge with positive potentials occuring over cations and negative potentials over anions, with the difference between the peaks depending on the degree of covalent (*vs.* ionic) bonding in the lattice (the greater the extent of covalent bonding the lower the difference between peaks). Occasionally, however, the chloride ion experiences vacancies, with cation vacancies appearing as sites of high negative charge (corresponding to a formal charge of $-\chi e$) and oxygen vacancies appearing as sites of high positive charge (formally $+2e$). Thus, the chloride ion is presented with a number of attractive sites to attack, but which will be favored? This is a difficult question to answer unequivocally, because other processes must be considered. For example, a chloride ion could absorb into a surface oxygen vacancy, but this must be done at the expense of considerable dehydration. However, the high coordination afforded by neighboring ions is a positive factor (favoring absorption), although any expansion of the vacancy to accommodate the ion would be energetically costly. The anion also could interact electrostatically with a positive center in the film surface represented by a surface cation; in this case, the interaction might be weaker (because of significant covalent bonding) but, because less dehydration is required in that the ion would not penetrate into the surface, the overall effect might favor absorption at a cation site. These two scenarios could lead to quite different mechanisms for localized attack.

In the first case (anion absorption into a surface oxygen vacancy), the film may respond in several ways (Fig. 7). In one way (case I), the system responds to the loss of oxygen vacancies by generating cation vacancy/oxygen vacancy pairs via a Schottky-pair type of reaction. The oxygen vacancies in turn react with additional anions (*e.g.*, chloride) at the film/solution interface to generate yet more cation vacancies. Importantly, the generation of cation vacancies is autocatalytic, but whether or not the film breaks down depends on the relative rates with which the cation vacancies are transported across the barrier layer and are annihilated by emission of cations from the metal into the film. If this annihilation reaction is incapable of consuming the cation vacancies arriving at the metal/film interface, the excess vacancies will condense and lead to the local detachment of the film from the underlying metal (Fig. 8). Consequently, provided the local tensile stresses are sufficiently high and/or the film dissolves locally (see below), the barrier layer will rupture, marking the initiation of a pit. The evidence for this mechanism is discussed later but, present at this picture is sufficiently encompassing to explore other processes that may occur in the barrier

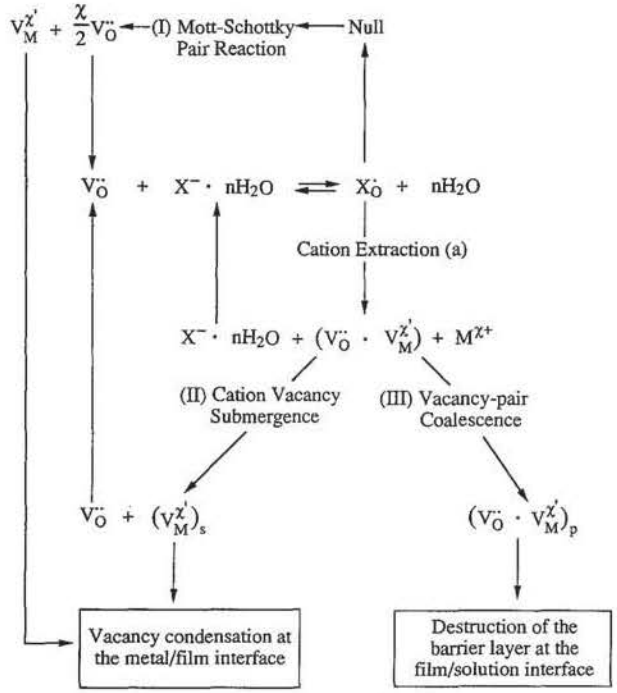

Fig. 7. Summary of proposed reactions leading to passivity breakdown.

layer as a result of anion absorption into a surface oxygen vacancy.

From Fig. 7, it is evident that an absorbed anion (*e.g.*, Cl^-) could desorb along with a surface cation to form a $(V_M^{\chi'}) \cdot (V_{\ddot{O}})$ pair [process a]. This process is perhaps favored in those cases where the anion has a tendency to complex with the cation (*e.g.*, in the case of iron in chloride solutions), rather than forming an insoluble compound, as in the case of silver in the presence of chloride ion. In any event, we proceed by exploring the fate of the vacancy pair. In one instance (case II), the cation vacancy may submerge into the barrier layer by the outward movement of a cation, resulting in the regeneration of an isolated surface oxygen vacancy. Because the anion vacancy may then absorb another anion, this process, too, is autocatalytic and has the additional feature that, because X^- is regenerated in the vacancy pair generation reaction (*i.e.*, reaction a) the concentration of absorbed anion ($X_{\ddot{O}}^{\bullet}$) may exist in a steady-state for any given set of conditions. Thus, reaction II leads to the anion-catalyzed generation of cation vacancies at the barrier layer/environment interface and to their penetration into the film. Clearly, the reaction will be favored at those (localized) regions of the film where the rate of penetration of the cation vacancies into the barrier layer is greatest. The submergence of cation vacancies into the barrier layer may not be favored; particularly in those films where the cation mobility is very low. In this case (reaction III), the $(V_M^{\chi'}) \cdot (V_{\ddot{O}})$ pairs may persist at the surface and eventually coalesce to destroy the lattice at the barrier layer/environment interface. It is not obvious, however, that reaction III should occur locally and hence result in pitting attack. More likely, reaction III represents macroscopic anion-catalyzed dissolution of the film, in a manner analogous to reaction 5 as depicted in Fig. 3.

To extend this argument we enquire where and how one might expect passivity breakdown to occur. Destruction of the barrier layer at the film/solution interface by vacancy pair formation is favored in those cases, or on those regions of the film, where cation mobility is very low. However, one expects the system to respond by growing additional film at the metal/film interface to satisfy Eq. 1. If this process occurs over a localized area then we expect the barrier layer to penetrate into the metal substrate in like fashion. This may be the mechanism of formation of porous anodic films on aluminum upon anodizing in acid solutions.[22] In this case, the barrier layer is scalloped in form, with each "scallop" subtending a pore. Presumably, dissolution (whether it be anion-catalyzed or not) occurs at some persistent defect that extends through the barrier layer to the film/solution interface. For films (or regions of films) where the cation mobility is high, destruction of the vacancy pairs by the outward flow of cations (inward flow of cation vacancies) is favored leading to the generation of cation vacancy condensates at the metal/film interface. Because pits are found to nucleate at points of high disorder (*e.g.*, at ghost grain boundaries, and at intersections of the film with inclusions and second phase particles), where high cation mobility is expected, the arguments presented above seem to favor vacancy condensate formation (cases I and II), rather than local film thinning (case III), as being the fundamental nucleation event, although local thinning is expected to occur, as argued below.

What are the consequences that vacancy condensation at the metal/film interface has for processes that occur at the film/solution interface? According to Eq. 1, for a film in the steady-state, a balance exists between the rate of film formation at the metal/film interface and the rate of dissolution at the film/solution interface. However, if the film is detached locally from the metal, due to the condensation of cation vacancies, then clearly reaction 2 shown in Fig. 3 cannot occur, so that the film ceases to grow into the metal. However, reaction 5 still proceeds, with the net effect that the film thins locally until rupture eventually occurs. Thus, a consistent picture emerges: passivity breakdown occurs at regions of the film that are characterized by high cation vacancy diffusivities. The first stage in this nucleation is the condensation of cation vacancies at the metal/film interface, causing local detachment of the film from the metal. As this occurs, due to inhibition of the generation of oxygen vacancies, at the metal/film interface and hence growth of the barrier layer into the metal, the film begins to

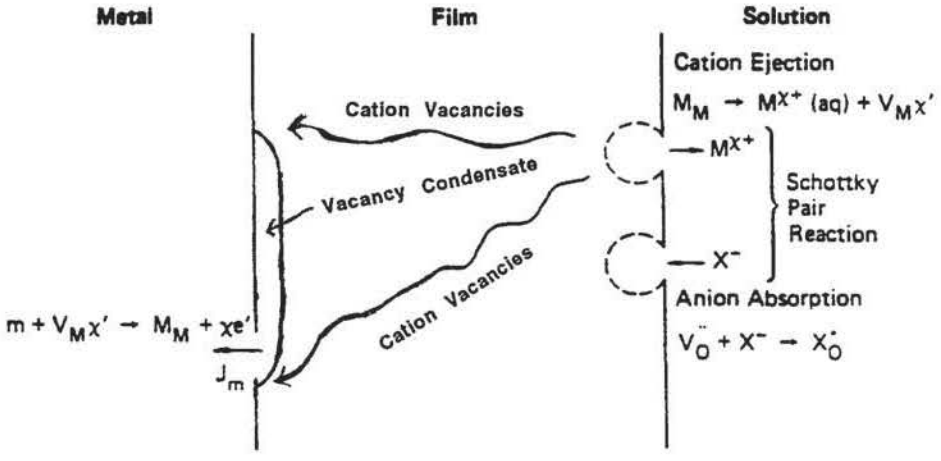

Fig. 8. One process leading to the breakdown of passive films according to the PDM.

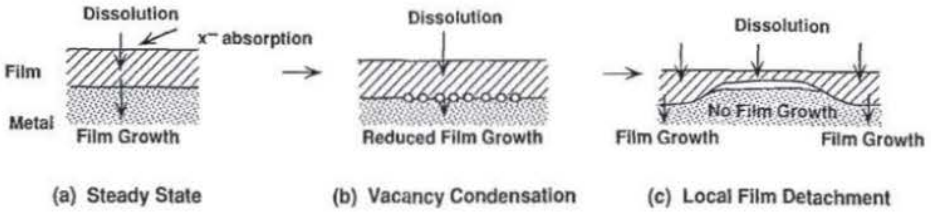

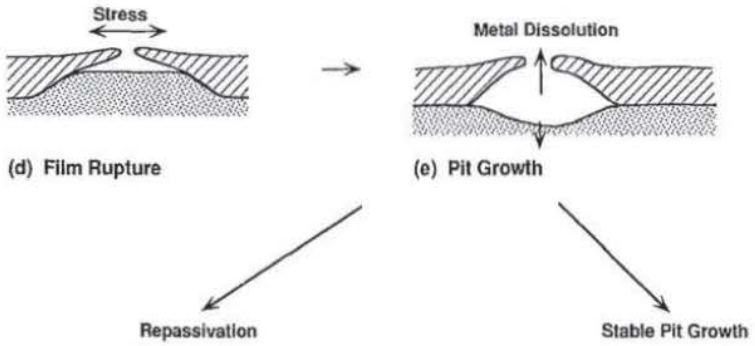

Fig. 9. Cartoon outlining various stages of pit nucleation according to the PDM.

thin due to the continued dissolution of the barrier layer by reaction 5 (Fig. 3). This will continue until rupture occurs, either due to complete dissolution or until mechanical rupture occurs because of residual or induced stresses. The various stages in pit nucleation, according to the above model, are depicted in the form of a cartoon in Fig. 9. As an operating definition of nucleation we include steps a, b, c, and d. Step e, and the subsequent fate of the nucleus, are not included in the nucleation event, as it is defined here.

Let me briefly summarize the evidence for vacancy condensation as the fundamental precursor for passivity breakdown. That vacancy condensates occur during the corrosion of steels in high-temperature aqueous environments[23] is seen readily from cross-sectional micrographs of the type shown in Fig. 10. In this case, not only has the barrier layer separated from the substrate metal, but voids, presumably formed by vacancy condensation, are evident in both the film and in the metal. The system depicted in Fig. 10 exhibited autocatalytic growth of magnetite on the metal surface, and displayed a corrosion rate of several meters per year! Accordingly, in this instance, the barrier layer supports an extraordinarily high cation vacancy flux, so that the detachment of the film from the metal and the appearance of vacancy condensates in the barrier layer and in the substrate metal are not surprising.

Clearly, the example cited above is extreme and the question remains as to whether vacancy condensation is a viable mechanism for passivity breakdown under less severe ambient conditions. In this instance, the direct observation of vacancy condensates (Fig. 10) is severely hampered by the small thickness of the barrier layer. Nevertheless, strong evidence exists in support of this mechanism.

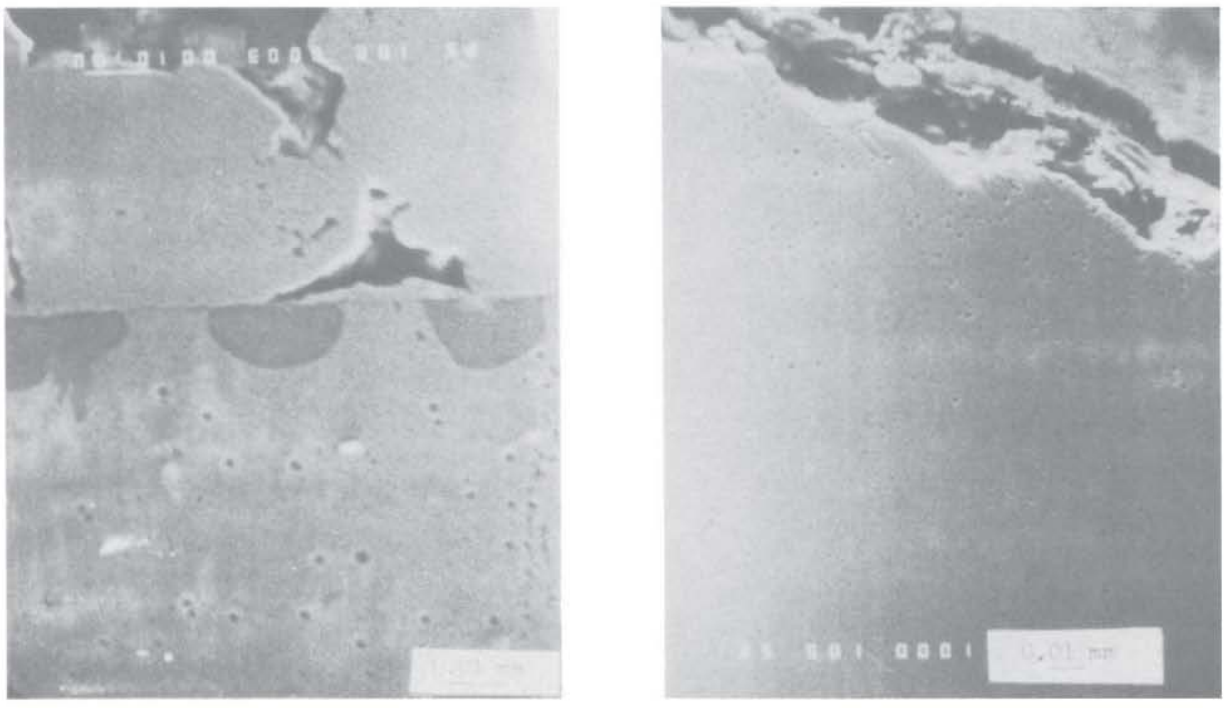

Fig. 10. Vacancy condensation in carbon steel after exposure to 0.80*M* NaCl + 0.1*M* $CuCl_2$ solution at 250°C for 62 h; (a, left) void nucleation in metal (lower) and oxide (upper); and (b, right) separation of barrier layer (upper right) from the metal substrate.

Thus, Givens *et al.*[24,25] found that the nucleation of pits on aluminum in chloride-containing solutions is preceded by the formaton of blisters which, of course, are local areas of detached film. The blisters grow with time and at some point emit a fine stream of bubbles (presumably hydrogen) prior to evident rupture. The potential at which blisters grew agreed well with the pitting potentials reported by Galvale and DeMicheli[26] and Foroulis and Thubrickar[27] for equivalent chloride concentrations over the range $[Cl^-]$ = 0.01 to 1.0*M*. In another study, Alwitt, Dyer, and Noble[28] examined Al_2O_3 anodic films on aluminum using transmission electron microscopy. While the anodic films were not grown in chloride-containing media (we argue later that chloride is not a necessary condition for vacancy formation), phase contrast effects in both amorphous and crystalline anodic films indicate the presence of voids that are 2-4 nm in diameter at apparent densities of 10^{11}-10^{12} cm^{-2}. Perhaps the most convincing evidence was obtained recently in the author's laboratory by graduate student Ellerbrock,[29] who showed that, while solid gallium is readily pitted in chloride containing media, liquid gallium (melting temperature = 29.78°C) does not suffer passivity breakdown readily as determined from potentiodynamic studies. This finding is consistent with the vacancy condensation hypothesis, because a condensate cannot exist at a liquid metal/film interface, whereas one can if the metal is solid. However, even this observation may not be unequivocal, because of the (expected) difference in stress state within a passive film on a liquid metal *vs.* that on a solid substrate.

The possibility that chloride ion (for example) might penetrate the barrier layer has been discussed extensively in the literature[15-17] on both theoretical and experimental grounds. The idea is attractive, because it could account for the induction time for pit nucleation, but on close examination the possibility that penetration of the barrier layer could occur seems remote. Numerous studies have shown that ionic conduction in metal oxides at near ambient temperatures is dominated by vacancy motion. Accordingly, it is highly unlikely that an anion the size of hydrated or even an unhydrated Cl^- (for example) could move through a metal oxide lattice (even a highly disordered one) interstitially. Therefore, if chloride penetration occurs, it has to be via the existing oxygen vacancy structure as $Cl_{\ddot{O}}^{\bullet}$ species (*i.e.*, as chloride ions occupying oxygen vacancies). However, $Cl_{\ddot{O}}^{\bullet}$ carries the same sign of charge as $V_{\ddot{O}}$ and, assuming the vacancies (including $Cl_{\ddot{O}}^{\bullet}$) to be ionized, any movement of chloride through the lattice would necessarily involve unfavorable transport up an electric potential gradient of the order of 10^6 V/cm. This is a most unlikely process, particularly since the flux of oxygen vacancies is irreversibly in the opposite direction. That chloride ions have been "found" in passive layers by techniques such as Auger electron spectroscopy is explained by their incorporation into the outer (precipitated) layer whose thickness may be many times that of the barrier layer, depending on the properties of the system, and by mixing due to (heavy ion, *e.g.*, Ar^+) bombardment during analysis. Alternatively, it could be postulated that chloride ions could move, as anionic species, through channels (*e.g.*, grain boundaries) in the film to the "bare" metal at the metal/film interface. However, presumably hydroxide ion could move likewise and, because of the much higher concentration of water (than chloride) at the barrier layer/solution interface, it is much more probable that such channels, in the unlikely event that they exist in the first place, would passivate.

In the analysis that follows, we assume that the initial event that occurs at the barrier layer/environment interface in passivity breakdown is the absorption of an aggressive anion (*e.g.*, Cl^-) into a surface oxygen vacancy

$$V_{\ddot{O}} + X^- \leftrightarrow X_O^{\bullet} \qquad [13]$$

followed by a Schottky-pair type reaciton

$$\text{Null} \rightarrow V_M^{\chi'} + \left(\frac{\chi}{2}\right) V_{\ddot{O}} \qquad [14]$$

as depicted in Fig. 7, Case I. In this mechanism, anion absorption leads to the generation of cation vacancies at the film/solution interface and hence to the increased flux of cation vacancies across the barrier layer. This particular case was considered in detail by Lin *et al.*,[3] who assumed that the enhanced flux of cation vacancies across the barrier layer, resulting from the increased concentration of vacancies at the film/solution interface according to reaction 14, could not be accommodated by reaction 1 in Fig. 3, thereby leading to the formation of a cation vacancy condensate. Once the condensate (Fig. 8) has grown to a critical size, dissolution of the film at the film/solution interface and the tensile stresses in the barrier layer induce a mechanical or structural instability, resulting in rupture of the film and hence in rapid localized attack. These ideas were assembled by Lin *et al.*[3] to derive expressions for the critical breakdown voltage and induction time for a single breakdown site as

$$V_c = \frac{4.606RT}{\chi F\alpha}\log\left[\frac{J_m}{J^\circ u^{-\chi/2}}\right] - \frac{2.303RT}{\alpha F}\log\left(a_{X^-}\right) \qquad [15]$$

and

$$t_{ind} = \xi'\left[\exp\left(\frac{\chi F\alpha\Delta V}{2RT}\right) - 1\right]^{-1} + \tau \qquad [16]$$

where ΔV is the breakdown overvoltage ($\Delta V = V - V_c$), a_{X^-} is the activity of X^- in the solution

$$\xi' = \xi/J^\circ u^{-\chi/2}\,(a_{X^-})^{\chi/2}\exp\left(\frac{\chi\alpha FV_c}{2RT}\right) \qquad [17]$$

and ξ is the critical areal concentration of cation vacancies at the metal/film interface. Other parameters are as defined in the original publication.[3] Equations 15 and 16 account for many of the phenomenological characteristics of pitting attack; (*i*) that the "pitting potential" (V_c) varies linearly with log (a_{X^-}) with a slope greater than $2.303RT/F$ (*i.e.*, > 0.05916 V/decade at 25°C) because $\alpha < 1$, (*ii*) that log (t_{ind}) α $1/\Delta V$ for sufficiently large overvoltages, and (*iii*) that t_{ind} is an inverse function of the activity of the aggressive anion.

In deriving Eq. 15 and 16, we have assumed that the critical concentration of cation vacancies at breakdown (ξ mol vacancies/cm^2) is independent of the applied voltage and hence thickness of the barrier layer. This assumption was made because transmission of cation vacancies through the film can occur only as long as the film is attached to the base metal such that the vacancies can be annihilated by reaction 1, Fig. 3 (also Fig. 8). Thus, growth of the condensate normal to the interface cannot occur, once the film has separated from the substrate, and since separation occurs by condensation of a single layer of vacancies our assumption of $\xi \neq f(V, L)$ is justified.

Why is chloride ion so effective at inducing passivity breakdown on many metals and alloys? An explanation is formulated in terms of the absorption of X^- into an oxygen vacancy, which may be represented as

$$X^- \cdot nH_2O + V_{\ddot{O}} \leftrightarrow X_O^{\bullet} + nH_2O \qquad [18]$$

The Gibbs energy for this reaction is composed of two principal components with regard to the identity of X; the dehydration energy ΔG_h° and the energy required to expand the vacancy to accommodate the ion (ΔG_e°). Thus, in moving along the series F^-, Cl^-, Br^-, and I^-, ΔG_h° becomes less positive due to the decreasing tendency of larger ions to hydrate but this is offset by the greater (more positive) energy that is required to expand the vacancy. Thus, the two contributions cross and preliminary semiquantitative calculations indicate that Cl^- has the most favorable Gibbs energy of absorption into an oxygen vacancy in NiO (for example). Of course, ΔG_e° depends on the size of the oxygen vacancy in the surface of the barrier layer; the larger the size, the more favorable is the Gibbs energy of absorption for the larger anions. Accordingly, depending on the size of the vacancy, other anions may be better able than chloride to induce passivity breakdown. For example, bromide apparently induces pitting in titanium at a lower voltage than does chlo-

ride,[30] possibly reflecting differences in oxygen vacancy size compared with nickel oxide.

On any real surface, a large number of potential breakdown sites exist corresponding to a distribution in the properties of the "weak spots." Perhaps the most graphic illustration of this property is the data of Shibata and coworkers,[31,32] who showed that the "pitting potential" is near normally distributed and that the induction time follows a distribution that is skewed toward short times. Assuming that the breakdown sites on a surface are normally distributed with respect to the cation vacancy diffusivity, we derived distribution functions for the breakdown voltage and induction time of the form[d] [9,10]

$$\frac{dN}{dV_c} = -\frac{1}{\sqrt{2\pi}\sigma_D \gamma D} e^{-(D-\bar{D})^2/2\sigma_D^2} \quad [19]$$

and

$$\frac{dN}{dt_{ind}} = \left[\frac{\xi u^{\chi/2}}{\sqrt{2\pi}\sigma_D \hat{a}}\right] e^{-(D-\bar{D})^2/2\sigma_D^2} \cdot \frac{e^{-\gamma V}}{a_\chi^{\chi/2}(t_{ind}-\tau)^2} \quad [20]$$

where $\gamma = \alpha\chi F/2RT$, σ_D is the standard deviation for the diffusivity for the population of breakdown sites, and the other quantities are as previously defined.[9,10]

For comparison with experiment, we define the cumulative probability in the breakdown voltage and the differential cumulative probability in the induction time as

$$P(V_c) = \frac{100 \int_{-\infty}^{V_c} \left(\frac{dN}{dV_c}\right) dV_c}{\int_{-\infty}^{\infty} \left(\frac{dN}{dV_c}\right) dV_c} \quad [21]$$

and

$$[\Delta N]_{t_j}^{t_{j+1}} = \int_{t_j}^{t_{j+1}} \left(\frac{dN}{dt_{ind}}\right) dt_{ind} \quad [22]$$

The latter quantity is defined in this manner so that direct comparison can be made with experimental pitting induction time data, which are commonly presented as histograms of the number of pits nucleating in successive increments of time.

A fit of $P(V_c)$ to the experimental data of Shibata *et al.*[31,32] for pitting of Fe-17Cr in 3.5% NaCl solution at 30°C is shown in Fig. 11. This fit was accomplished by adjusting groups of unknown or poorly-known parameters, which affect the location of $P(V_c)$ on the potential axis but not the shape, such that the experimental and calculated distribution functions coincide for a mean diffusivity for cation vacancies of 5×10^{-20} cm^2/s (this is approximately the value indicated by electrochemical impedance spectroscopy). Without adjusting any additional parameters, the distribution (histogram) in induction time agrees with the experimental data for the same system (Fig. 12). The model described thus far does not consider the "death" or repassivation of pits; however, its omission is appropriate because, in Shibata's analyses, each specimen was taken out of the population once breakdown had occurred. Similar distributions in V_c and t_{ind} are obtained if we assume other distribution functions (*e.g.*, the student-t and χ^2 distributions) for the breakdown sites with respect to cation vacancy diffusivity.

[d] Equations 21 and 22 are given in slightly different form in Ref. 9 and 10.

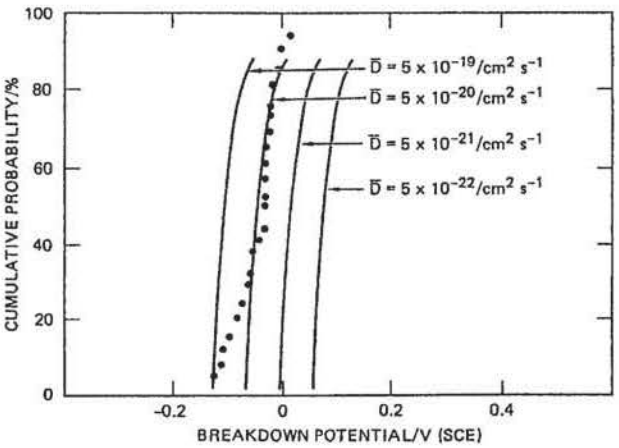

Fig. 11. Cumulative probabilities for the breakdown voltage as a function of D for normal distributions in the diffusivity D. $\sigma_D = 0.75$. Data for Fe-17Cr in 3.5% NaCl solution at 30°C from Shibata,[31,32] $V_c = -0.046$ V (SCE).

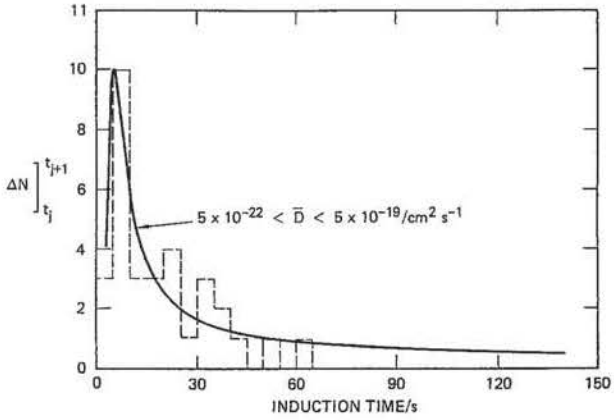

Fig. 12. Differential cumulative probabilities for the induction time as a function of $\bar{D}$ for normal distributions in D. $\sigma_D = 0.75$ $\bar{D}$. (----) Data for Fe-17Cr in 3.5% NaCl solution at 30°C from Shibata.[31,32] $V_c = -0.046$ V (SCE), $V = 0.020$ V (SCE), $t = 7.5$ s, $\tau = 0$.

The analysis outlined above has permitted us to identify factors that make for "good passivity." Besides lowering the total number of potential breakdown sites per unit area of the surface, the parameter that may be manipulated to impact the susceptibility of a passive film to chemically induced breakdown is the cation vacancy diffusivity. Thus, a decrease in the cation vacancy diffusivity results in an increase in the "pitting potential" (*i.e.*, $\bar{V}_c$), because a higher voltage is required to produce the same flux of cation vacancies across the barrier layer. Note that metals that have inherently low cation vacancy diffusivities (*e.g.*, Ti, Zr, Ta) are quite resistant to pitting.

An important application of the idea that the cation vacancy diffusivity plays a central role in determining a system's (metal or alloy) susceptibility to pitting was developed some time ago by Urquidi-Macdonald and Macdonald[11] to explain the role of alloying elements in modifying the pitting resistances of alloys. The premise of this model [the solute-vacancy interaction model (SVIM)[12]] is that pairing occurs between highly charged solute (alloying element) ions substitutionally present in the barrier layer and mobile cation vacancies. Thus, molybdenum segregated into the barrier layer on a Ni-Mo alloy is presumed to be present as $Mo_{Ni}^{4\cdot}$ (*i.e.*, as a Mo^{6+} ion substituted into a nickel vacancy), which appears formerly as a center of four positive charges. That alloying elements are segregated into barrier layers (but not necessarily into the upper, precipitated layers) is shown unequivocally by the surface analysis by laser ionization (SALI) data presented in Fig. 13.[33] These data show that, for a series of Ni-X alloys, with X = Al, Ti, and Mo, the extent of segregation of the alloying element into the barrier layer increases with increasing charge on the solute (*i.e.*, Ni-Al < Ni-Ti < Ni-Mo, for which the solutes may be represented as $Al_{Ni}^{\cdot}$, $Ti_{Ni}^{2\cdot}$, and $Mo_{Ni}^{4\cdot}$). Furthermore, it is evident from the existence of the diffusion gradient of the alloying element in the alloy phase that segregation occurs via a solid-state reaction at the metal/film interface. This is consistent with the barrier layer on nickel being essentially a cation conductor, in which case segregation of the alloying element into the film can be described by the reaction

$$A + V_{Ni}^{2'} \rightarrow A_{Ni}^{x} + (x+2)e' \quad [23]$$

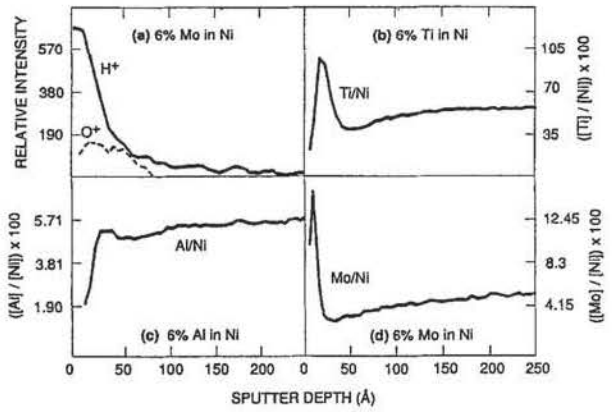

Fig. 13. Concentration profiles of H, O, Al, Ti, and Mo in passive films formed on Ni-6% Al, Ni-6% Ti, and Ni-6% Mo in 0.1*N* H_3PO_4/NaOH, pH = 12, at 25°C as determined by surface analysis by laser ionization. *V* = 0.30 V *vs.* SCE.[33]

in completion with the injection of host cations into the film

$$Ni + V_{Ni}^{2'} \rightarrow Ni_{Ni} + 2e' \qquad [24]$$

The greater segregation of more highly charged solutes into the barrier layer can be explained in terms of their more favorable free energy in the high dielectric film [for example, experimental measurements indicate that the dielectric constant for the passive film on Cr is ≈56 whereas that on Type 304SS is 68-107, see citations in Ref. 11].

Returning now to the role of alloying elements in passivity breakdown, we proposed[11] that the interaction between the substitutionally present (immobile) solute and mobile cation vacancies can be represented as a chemical equilibrium

$$A_M^{(n-\chi)+} + qV_M^{\chi'} \overset{K_q}{\longleftrightarrow} [A_M(V_M^{\chi'})q]^{[n-\chi(1+q)]\cdot} \qquad [25]$$

where n is the oxidation charge of the solute (*e.g.*, +6 for Mo^{+6}), and K_q is the equilibrium constant. For example, if M is nickel, A is molybdenum, and $q = 1$, the association reaction can be written as

$$Mo_{Ni}^{4\cdot} + V_{Ni}^{2'} \leftrightarrow (Mo_{Ni} \cdot V_{Ni})^{2\cdot} \qquad [26]$$

Clearly, further complexing could occur

$$(Mo_{Ni} \cdot V_{Ni})^{2\cdot} + V_{Ni}^{2'} \leftrightarrow [Mo_{Ni} \cdot (V_{Ni})_2] \qquad [27]$$

to form a neutral species. Evidently, not only is the strength of the electrostatic interaction between the solute and a mobile cation vacancy greater for more highly charged solutes, but the total number of vacancies that may be complexed is also greater. The effect of complexing is to decrease the diffusivity and concentration of mobile cation vacancies in the film, all other factors remaining the same. For 1:1 complexes, Urquidi-Macdonald and Macdonald[11] derived the modified vacancy diffusivity as

$$D^* = \frac{D}{2}\left[1 \mp \frac{(\hat{\alpha} - n_A)}{(\hat{\alpha}^2 - n_A n_V)^{1/2}}\right] \qquad [28]$$

and a modified K^* ($=\varepsilon F/RT$) as

$$K^* = 2K\frac{[1 - \hat{\alpha}/n_V \mp (\hat{\alpha}^2 - n_A n_V)^{1/2}/n_V]}{[1 \mp (\hat{\alpha} - n_A)/(\hat{\alpha} - n_A n_V)^{1/2}]} \qquad [29]$$

where $\hat{\alpha} = (n_A + n_V + K_1^{-1})/2$, and n_A and n_V are the stoichiometric concentrations of the solute and cation vacancies in the film. By applying ion-pairing theory, as used in solution theory and in solid state physics, we can express the equilibrium constant, K_1, as

$$K_1 = \left[4\pi(t/kT)^3 \int_2^{t/akT} e^{\gamma}\gamma^{-4}\, d\gamma\right] \qquad [30]$$

where a is the distance of closest approach, $t = |z_1 z_2| e^2/\hat{\varepsilon}\hat{\varepsilon}_o$, z_1 and z_2 are the number of charges on the interacting species, e is the electron charge, $\hat{\varepsilon}$ is the dielectric constant, $\hat{\varepsilon}_o$ is the permittivity of free space, and γ is the variable of integraton. The equilibrium constant, K_1, needs to be corrected for screening by the mobile vacancies. This correction is expressed through Debye-Huckel theory as[11]

$$K_1^{corr} = K_1 f_A f_M \qquad [31]$$

where f_A and f_M are activity coefficients given by

$$f_A = \exp\left\{-\frac{e^2(n - 2\chi)^2}{2\hat{\varepsilon}\hat{\varepsilon}_o T \ell_D (1 + b'/\ell_D)}\right\} \qquad [32]$$

and

$$f_M = \exp\left\{-\frac{e^2\chi^2}{2\hat{\varepsilon}\hat{\varepsilon}_o kT \ell_D (1 + b'/\ell_D)}\right\} \qquad [33]$$

where ℓ_D is the Debye length

$$\ell_D = \left\{\frac{\hat{\varepsilon}\hat{\varepsilon}_o kT}{e^2 4\pi[n_V\chi^2 + n_A(n - 2\chi)^2]}\right\}^{1/2} \qquad [34]$$

and b' is the distance at which the coulombic interaction energy is equal to kT (the thermal energy)

$$b' = \frac{\chi(n - 2\chi)e^2}{2\hat{\varepsilon}\hat{\varepsilon}_o kT} \qquad [35]$$

Although the SVIM is currently quite crude, in that it does not consider the complexing of more than one cation vacancy per solute and does not employ exponential distributions of vacancies across the film, the model is surprisingly successful in accounting for the effect of molybdenum, for example, on the pitting characteristics of stainless steel. Thus, by combining the SVIM with the distribution functions for passivity breakdown, we calculated $P(V_c)$ as a function of molybdenum concentration in the alloy, assuming that the solute is in the +6 oxidation state (we also have considered the +4 state but it will not be discussed extensively here) and that preferential segregation of Mo into the barrier layer did not occur (*i.e.*, the concentration of Mo in the barrier layer was assumed to be the same as that in the base alloy). The distribution functions are shown in Fig. 14. In deriving these data, we selected model parameters so that the molybdenum-free case coincided with the experimental data of Shibata[31,32] for Fe-17Cr in 3.5% NaCl at 30°C; these parameters were then maintained constant for all molybdenum-containing alloys. Accordingly, as far as the latter are concerned, there are no arbitrarily adjustable parameters in the model.

The $P(V_c)$ data plotted in Fig. 14 predict that small additions of molybdenum (*e.g.*, 1%) have only a modest impact on the pitting characteristics of stainless steel, but that additions of greater than 2% have a large impact. However,

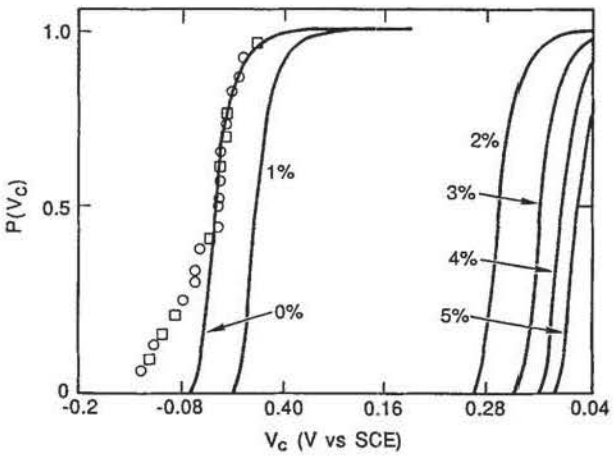

Fig. 14. Effect of solute (Mo) concentration (n_{Mo} · w/o) on the cumulative distribution function for V_c for a passive film containing 6^+-3 complexes. $n_V = 5 \times 10^{20}$ cm^{-3}, $K_1 = 1.13 \times 10^{-16}$ cm^3. (○, □) Data of Shibata[31,32] for Fe-17Cr in 3.5% NaCl at 30°C.

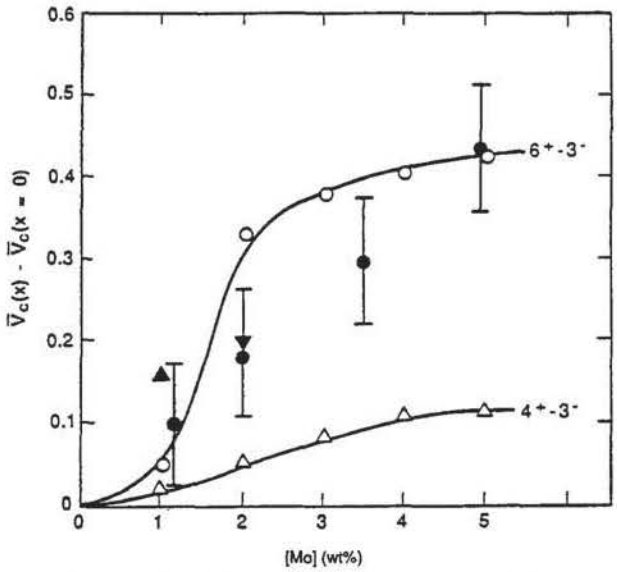

Fig. 15. Effect of molybdenum concentration on $V_c(x) - V_c(x=0)$ for 6^+-3^- (○) and 4^+-3^- (△) complexes in the film. $n_V = 5 \times 10^{20}$ cm^{-3}, $K_1 = 1.13 \times 10^{-16}$ cm^3 (○), $K_1 = 9.05 \times 10^{-21}$ cm^3 (△). (●) Lislovs and Bond[34]: Fe-18Cr in 1M NaCl at 25°C. (▲) Shibata[31]: Fe-17Cr in 3.5% NaCl at 30°C. (▼) Shibata[32]: Fe-18Cr in 3.5% NaCl at 30°C.

additions of more than 3% have incrementally smaller effects. Experience has shown that 2-2 1/2% Mo is optimal for protecting Type 304SS against pitting in seawater systems with the modified alloy being the well-known Type 316SS. Perhaps a better test of the SVIM is afforded by the data plotted in Fig. 15, where a comparison of $\bar{V}_c$ (breakdown voltage at the 50th percentile) is made with experimental data from the literature. Although the experimental data do not display the sigmoid shape predicted by theory (and probably could not because of their limited precision), the agreement between experiment and theory is surprisingly good. Also shown is the prediction of the SVIM assuming that molybdenum is in the +4 state; clearly, the former (Mo^{6+}) provides a better description of the experimental data than does the latter (Mo^{4+}), although the actual oxidation state of molybdenum in the barrier layer on stainless steel has not been established unequivocally. The major impact of shifting $P(V_c)$ in the positive direction is to greatly increase the induction time for passivity breakdown (*i.e.*, the time required to accumulate a critical concentration of cation vacancies at the metal/film interface). Although we do not show the calculations here, this is precisely what is predicted by the model.

Other data also support the predictions of the model. For example, various studies[35-37] on supersaturated aluminum alloys of the type Al-X (X = 0-8 a/o Mo, Cr, Ta, W) have shown that elements such as molybdenum and, in particular, tungsten can displace the critical potential for pitting in chloride solution in the positive direction by as much as 2.6*V*. Both elements form species in the +6 oxidation state, which should complex mobile $V_{Al}^{3\bullet}$ vacancies, although the extensive segregation of the alloying element into the barrier layer has not been demonstrated. However, in the presence of a thick outer layer (relative to the barrier layer), even when using a glancing radiation technique (*e.g.*, EXAFS) as employed in those studies,[35-37] it is difficult to establish the extent of segregation into the barrier layer alone, and it is likely that techniques with much higher depth resolution, such as SALI, are required to fully characterize the composition of the interfacial region.

Transpassive dissolution and electropolishing.—In the case of pitting corrosion, we have argued that passivity breakdown occurs locally (probably on the micron or submicron scale) because of anion-catalyzed cation vacancy generation at the barrier layer/solution interface (Fig. 9). Breakdown, and hence pit nucleation, is envisioned to occur at "weak spots" that are characterized by high cation vacancy diffusivities. These sites include those where structural discontinuities exist in the barrier layer, such as at ghost-grain boundaries projecting through the film from the metal or alloy substrate, and at the boundaries between the barrier layer and inclusions. The fundamental event leading to breakdown is envisioned to be cation vacancy condensation at the metal/film interface, which leads to decohesion of the barrier layer from the metal and ultimately to film rupture because of the presence of tensile stresses in the film coupled with film dissolution.[38-42]

While we have focussed our attention on anion-catalyzed generation of cation vacancies at the barrier layer/solution interface, other processes may lead to a sufficiently high rate of generation of cation vacancies that film breakdown can occur in the absence of "aggressive" anions. Thus, increasing the potential results in an accelerated ejection of cations from the film according to reaction 3 (Fig. 3). For the particular case of the stainless steels, we envision the generation of cation vacancies by the reaction (cf. reaction 3, Fig. 3)

$$Cr_{Cr} + 4H_2O \rightarrow CrO_4^{2-} + V_{Cr}^{3'} + 8H^+ + 3e'$$

in which Cr_{Cr} represents a Cr^{3+} cation in the passive film lattice. The rate of this reaction is a strong function of potential. Accordingly, at a sufficiently high potential, the cation vacancies so generated cannot be annihilated by reaction 1, the rate of which is only weakly dependent on the applied voltage because of the high value of α (Eq. 4). However, unlike the pitting case, where anion-catalyzed generation of cation vacancies is most prevalent at those sites where cation vacancies most rapidly submerge into the film, we see that condensation of cation vacancies at the metal/film interface occurs generally across the surface, thereby leading to the macroscopic decohesion of the barrier layer from the metal (Fig. 9). Once breakdown has occurred over macroscopic areas, the high (mass-transport-controlled) dissolution rate of the substrate will inhibit the formation of the barrier layer although, of course, an outer layer may form, possibly as a "salt film."[43] Accordingly, the system does not passivate in the sense of the passivity (due to the formation of a barrier layer) that exists at lower potentials in the passive range (Fig. 16), but nevertheless, the current decreases with time due to mass transfer through the establishing outer layer. This, then is the mechanism we offer for the phenomenon of transpassive dissolution and electropolishing, both of which involve the

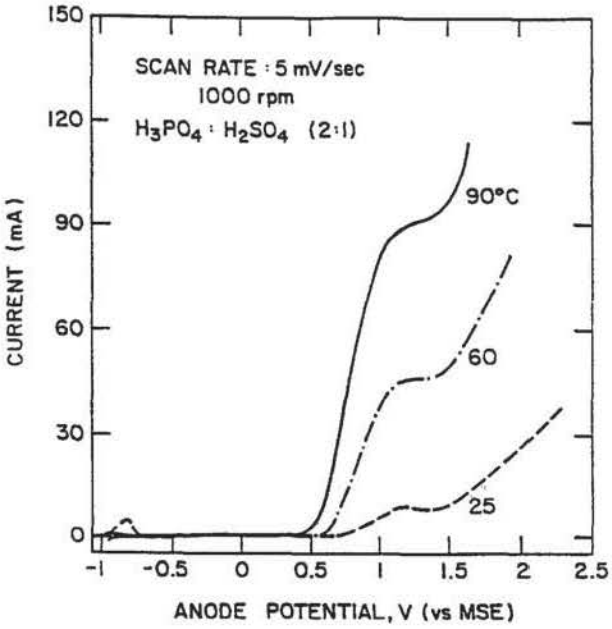

Fig. 16. The influence of electrolyte temperature on the polarization behavior of 420 stainless steel in a mixture of 2 parts by volume of phosphoric acid and one part of sulfuric acid.[45]

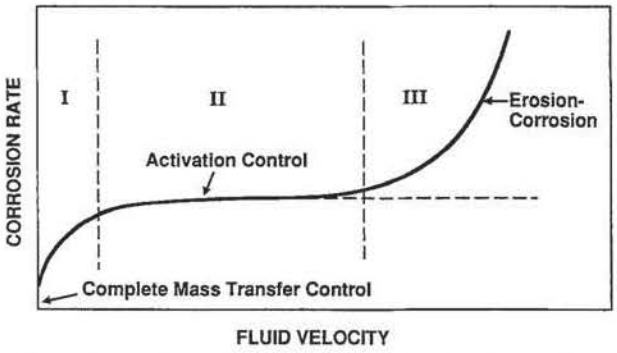

Fig. 17. Schematic variation of corrosion rate with fluid velocity.

breakdown of passivity across macroscopic areas at high applied potentials.[44-46]

Erosion/corrosion.—Erosion-corrosion[47,48] is the phenomenon where passivity breakdown is induced by the relative flow of the environment with respect to the metal. Phenomenologically, the corrosion rate suddenly increases at a critical flow velocity (Fig. 17), leading to the common explanation that this is the velocity at which the shear stress at the interface is sufficient to "strip" the passive film from the surface. However, as pointed out by Syrett,[48] the shear stresses appear far too low to induce mechanical rupture alone; therefore, we must inquire into the effect of fluid flow on the electrochemical properties of the interface in formulating a model for erosion-corrosion.

In the case of copper/nickel alloys in flowing oxygenated seawater,[49-51] the corrosion potential increases with increasing flow velocity, which is attributed to enhanced mass transport of oxygen to the alloy surface. However, at the critical velocity, the corrosion potential is close to that for transpassive dissolution in quiescent systems.[49] Cation vacancy condensation seems to account for electropolishing and transpassive dissolution in erosion-corrosion in the case of copper-nickel alloys. In this model erosion-corrosion is best attributed to flow-induced decohesion of the barrier layer, in which relatively low shear stresses are required to depassivate the surface due to condensation of cation vacancies at the metal/barrier layer interface. As in the case of transpassive dissolution, the metal surface is not necessarily "bare" because the rapid hydrolysis of cations leaving the surface results in the existence of a precipitated (salt) layer (Fig. 2).

This model for erosion-corrosion accounts for some important observations, including that erosion-corrosion is greatly inhibited by the addition of small amounts of alloying elements, such as chromium (Fig. 18), to the alloy.[52] The effective alloying elements are those that can form highly charged solutes in the barrier layer, and it seems reasonable to attribute inhibition of erosion-corrosion to complexing between the immobile solute and mobile cation vacancies, as we have proposed above for pitting corrosion. Interestingly, in the case of iron in high-temperature water,[47] erosion-corrosion is inhibited by increasing concentration of oxygen in the environment. This observation appears in conflict with the prediction of the model outlined above, until we note that increasing oxygen is expected to increase the concentration of Fe(III) in the film. Accordingly, the ferric species may act as the "highly charged solute," in the same manner as does Cr(III) or Cr(VI) in the passive film on Cu-Ni alloys, thereby inhibiting the movement of $V_{Fe}^{2'}$ across the barrier layer.

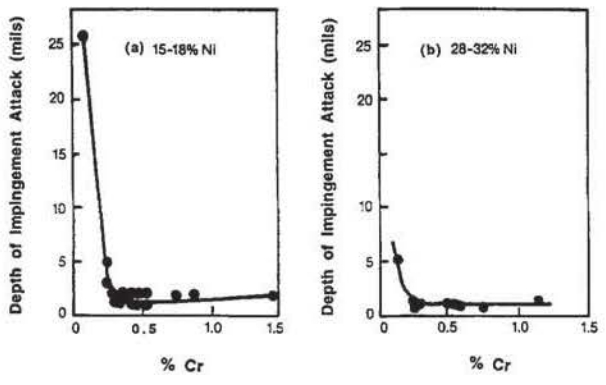

Fig. 18. Effect of chromium additions on seawater impingement—corrosion resistance of copper-nickel alloys. 36-day test with 7.5 m/s jet velocity; seawater temperature: 27°C.[52]

Alloy Design

What makes a good alloy? An answer to this question is of enormous scientific, technological, and economic importance, given that the annual cost of corrosion in any industrial society is about 4.5% of the GNP (about $230 billion for the US in 1990). The work outlined above provides clear guidance on this question and, recognizing that the models are still crude, we have formulated a set of principles to aid the alloy designer in devising new systems of superior resistance to passivity breakdown. The rules are as follows

1. The alloying element must segregate into the barrier layer, preferably preferentially with respect to the host cation.
2. The alloying element must exist in an immobile "dissolved" state in the barrier layer in as high an oxidation state as possible and certainly in an oxidation state that is higher than that of the host cation.
3. The alloying element should be uniformly distributed throughout the layer or at least should not form a second phase that would introduce heterogeneities into the system (and hence, sites for pit nucleation).

We have tested these principles by measuring distribution functions, $P(t_{ind})$, for a series of Ni-xAl, Ni-xTi, and Ni-xMo alloys (x = 0-8 atomic percent) in NaCl/borate buffer solutions at 25°C.[53] In these experiments, the specimens were held at a constant potential above the "pitting potential," and the number of pits nucleated on the surface were counted as a function of time. Although these experiments are complicated by the observation that existing active pits protect the remaining surface at radii that increase with time (and for this reason they have not been published), the data are in good qualitative agreement with the predictions of the model, in that the Ni-Mo alloys were the most resistant and the Ni-Al alloys were the least resistant to passivity breakdown, with the effect being roughly in proportion to the charge on the solute (*i.e.*, 4:2:1 for Mo_{Ni}^{4}:Ti_{Ni}^{2}:Al_{Ni}).

Photoinhibition of Passivity Breakdown

In the above discussion, we attribute inhibition of passivity breakdown to the binding of mobile cation vacancies to immobile solutes in the barrier layer, the net effect being a lowering of the flux of vacancies across the film. There is, however, one other way of lowering the flux and that is to decrease the electric field strength. However, we have noted that the electric field strength is independent of the applied voltage and the barrier layer thickness, so that manipulation of these parameters does not allow us to affect the desired change. However, the photogeneration of electron/hole pairs within the film should quench the electric field, and this effect has a strong influence on the nucleation of pits on nickel in chloride-containing solutions.

Photoinhibition of passivity breakdown was found accidently in my laboratory by Lenhart,[54] who was attempting to measure distribution functions for the nucleation of pits on nickel in chloride solutions using an electrochemical cell under an illuminated stage of a microscope. He found the results (number of pits *vs.* time) to be completely irreproducible, until we noted that the distribution function obtained depended on the setting on the power supply of the illuminating lamp! By varying the power to the lamp, we obtained almost complete photoinhibition of pit nucleation at relatively low power levels of white light (8 mW/cm^2) (Fig. 19). The explanation for the effect is readily gleaned

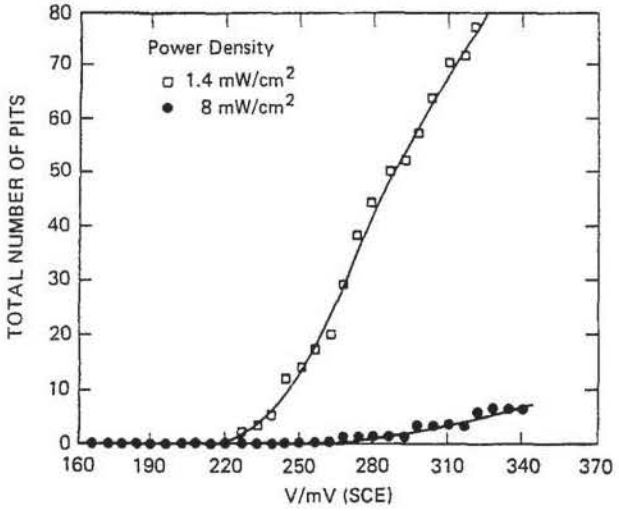

Fig. 19. Cumulative distribution for the inhibition of pits on nickel in 2M NaCl/0.1M KOH + 0.2M $B(OH)_3$ (pH = 9.2).

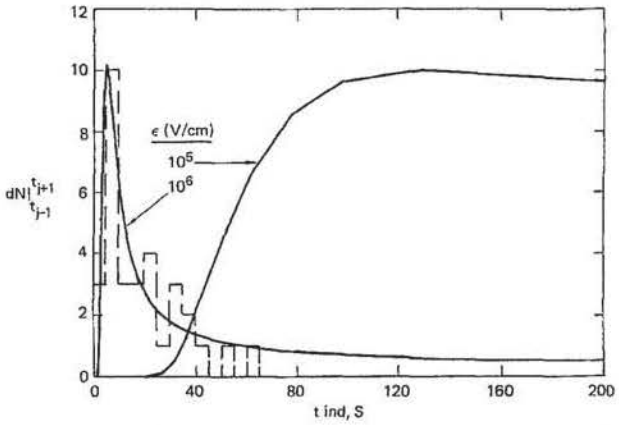

Fig. 21. Calculated distributions in the induction time for the breakdown of passive films as a function of electric field strength ε. β = −0.01, a_x = 0.042, T = 298 K, pH = 7, $D = 5 \times 10^{-20}$ cm²/s, σ_D = 0.75D. (— — —) Data from Shibata for Fe-17Cr in 3.5% NaCl solution at 30°C.[31,32]

from the PDM (Eq. 19, 20), which shows that the $P(V_c)$ and $P(t_{ind})$ are shifted to higher voltages and longer times, respectively, as the electric field strength is decreased. As shown in Fig. 20 and 21, a decrease in the field strength by a factor of ten is expected to shift the distribution in the breakdown voltage by a modest amount (~70 mV), but the shift in the induction time distribution is very large. Indeed, the observed degree of photoinhibition shown in Fig. 19 can be simulated by decreasing the electric field strength by a factor of less than ten.

Because stress corrosion cracks in steam-cycle components frequently nucleate at pits, photoinhibition promises to be an effective method of preventing fracture in thermal and nuclear power plants. This corrosion protection technology is being explored in our laboratory currently.

Prediction of Corrosion Damage Functions

A principal goal in corrosion science and engineering is the prediction of damage functions for various forms of corrosion as a function of exposure time. If this goal can be met, a rational deterministic basis might be established for estimating component lifetimes in industrial systems. Of great importance is the damage function for pitting corrosion, examples of which are shown in Fig. 22 for Type 403SS before and after being buried in the ground for five years.[55] Because this form of attack frequently leads to failure without significant outward signs of corrosion, the scheduling of preventative maintenance in industrial systems prone to this form of damage is an extremely difficult task. The PDM may provide the necessary deterministic basis for predicting localized corrosion damage functions, and hence for scheduling maintenance, as outlined below.

Consider the cumulative probability function for the induction time (integral of Eq. 21) as shown schematically in Fig. 23a. For an increment $\Delta t = t_{j+1} - t_j$, a total of $\Delta N]_{t_j}^{t_{j+1}}$ pits nucleate and grow for a period u before being observed at t_{obs}. If the rate of growth during this period is $r(t)$, then these pits will grow to a depth of

$$h = \int_o^u r(t)dt \qquad [36]$$

Thus, by carrying out this calculation for all time increments $(t_{j+1} - t_j)$, we are able to construct the damage function for the time of observation, t_{obs}, as shown in Fig. 23(b). The observation time is now changed and the procedure outlined above is repeated to generate a family of damage functions corresponding to different times of observation in the future. Designating the damage function as

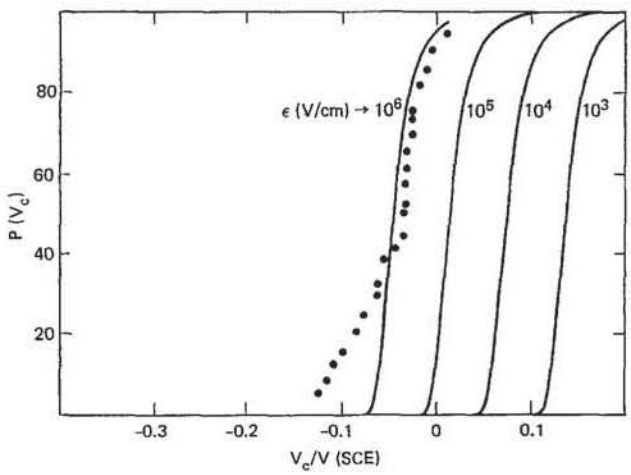

Fig. 20. Calculated distributions for the breakdown of passive films as a function of electric field strength ε. β = −0.01, a_x = 0.402, T = 298 K, pH = 7, $D = 5 \times 10^{-20}$ cm²/s, σ_D = 0.75D. (●) Data from Shibata for Fe-17Cr in 3.5% NaCl solution at 30°C.[31,32]

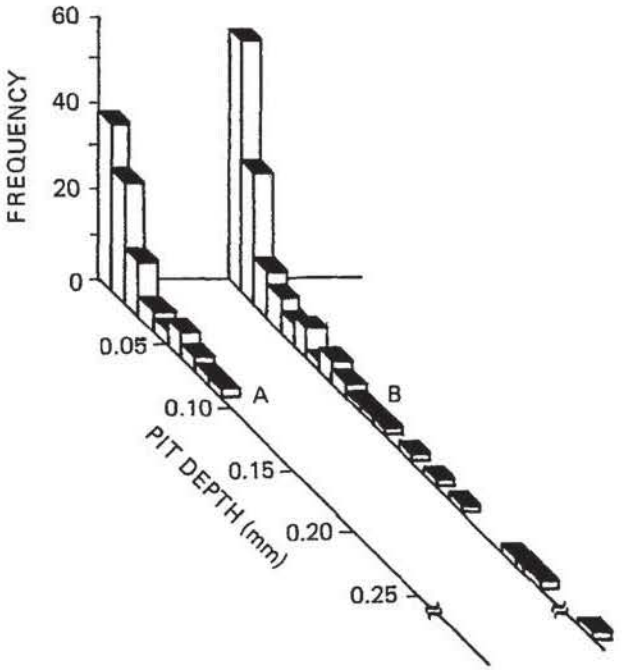

Fig. 22. Pit depth distributions for Type 403 stainless steel (After Ishikawa *et al.*[55]) A. Initial distribution; B. After five years.

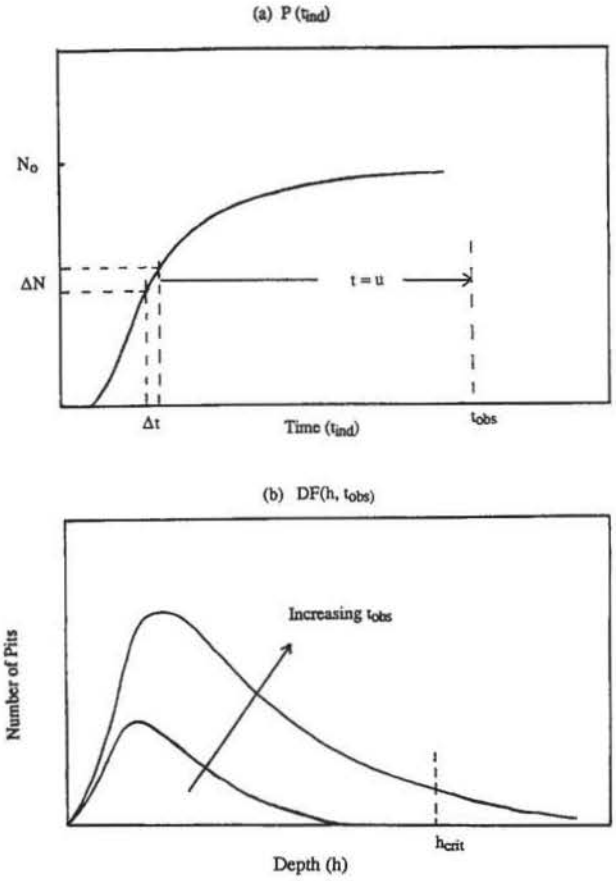

Fig. 23. Schematic of algorithm for calculating localized corrosion damage function, $DF(h,t_{obs})$ from the cumulative probability function for nucleation, $P(t_{ind})$.

$DF(h, t_{obs})$, we may calculate the probability of failure, $[PF(t_{obs})]$, defined as the probability that a pit will exceed in depth some critical dimension (h_{crit}, Fig. 23) as

$$PF(t_{obs}) = \frac{100 \int_{h_{crit}}^{\infty} DF(h,t_{obs})dh}{\int_{0}^{\infty} DF(h,t_{obs})dh} \quad [37]$$

which corresponds to the area beneath the damage function for $h > h_{crit}$ divided by the total area. The value of h_{crit} corresponds to some critical dimension selected on an engineering basis, such as the thickness of a pipe wall. Note that, in the analysis outlined above, we have not allowed for the repassivation ("death") of localized corrosion events; however, by modifying the cumulative probability function we allow for the possibility that a pit may repassivate at some time after nucleation.

Currently we are developing the algorithm outlined above to estimate damage functions for pitting corrosion on condensing heat exchangers in domestic and gas-fired furnaces and for stress corrosion cracking in water cooled nuclear reactors. In each case, we employ deterministic models to estimate pit and crack growth rates, respectively; these models are based on either Beck and Alkire's[56] diffusion model (for pit growth) or on the coupled environment fracture model (CEFM) that we developed previously to describe crack growth in sensitized Type 304SS in light-water-reactor-heat-transport environments.[57] Determinism is assured in the CEFM through charge conservation, by requiring that the net positive current exiting the crack (or pit) be consumed quantitatively on the external surfaces by appropriate cathodic reactions, such as oxygen reduction.

Typical examples of calculations of this type using the mass transport model of Beck and Alkire[56] for pit growth

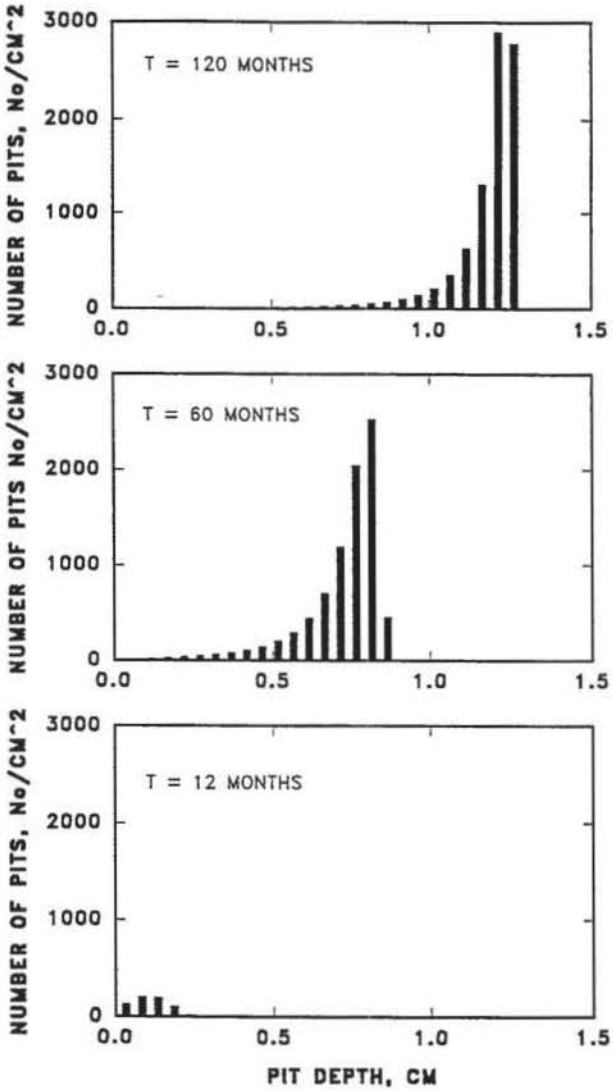

Fig. 24. Calculated damage functions for pitting corrosion as a function of time of observation. V_{app} = –0.275 V, V_c = –0.548V, $[Cl^-]$ = 6.3×10^{-4} mol/cm^3, $D = 5 \times 10^{-19}$ cm^2/s. Values for other parameters are given in Table II.

and the parameter values given in Table II are shown in Fig. 24 and 25. As expected, the form of the damage function depends significantly on the time at which it is observed (Fig. 24) with the pits extending to greater depths as the time of observation is extended into the future. The damage function also depends on the voltage at which the system is held (Fig. 25). In this case, the voltage dependence resides entirely in the nucleation function because the pit-growth model used in these calculations[56] does not admit to any potential dependence. Various shapes for the damage function may be generated simply by changing parameter values to alter the relative importance of nucleation *vs.* growth.

If the techniques outlined above can be developed successfully, they could be used to address the question of component lifetime prediction in three ways: (*i*) prediction of the minimum critical dimension for a given exposure time (t_{obs}) and probability of failure (PF); (*ii*) prediction of the service life of a component for a given critical dimension and probability of failure; and (*iii*) prediction of the probability of failure for a given critical dimension and exposure time.

All three modes are important to design and operations engineers, because they provide necessary inputs for selecting component dimensions [Mode i], for estimating component lifetime [Mode ii], and for scheduling maintenance [Mode iii]. The deterministic nature of the algorithm

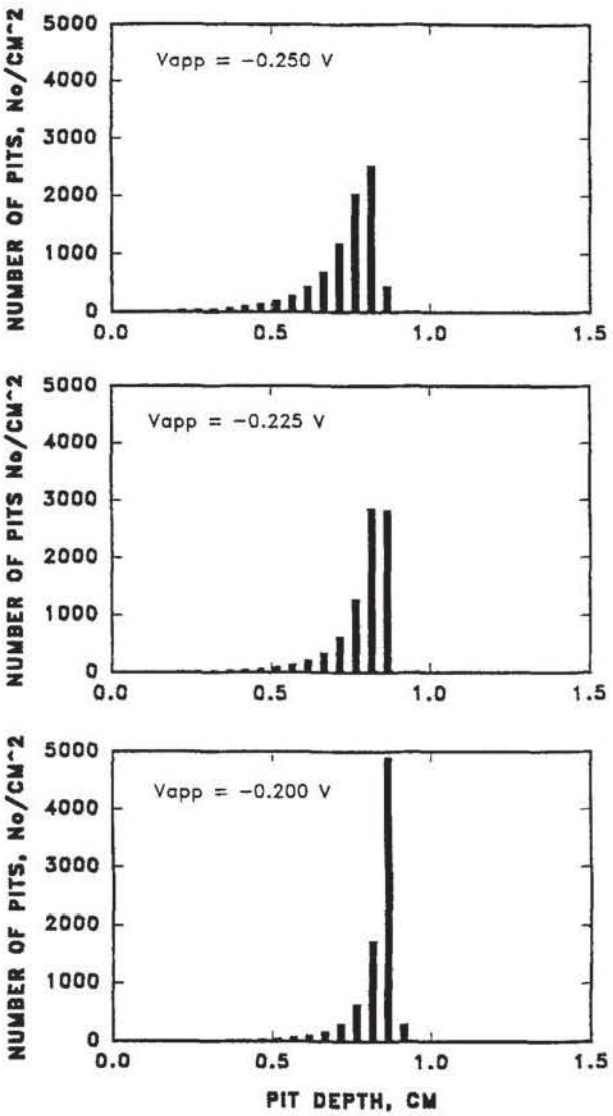

Fig. 25. Calculated damage functions for pitting corrosion as a function of applied voltage for a time of observation of 60 months. $V_c = -0.548$V, $[Cl^-] = 6.3 \times 10^{-4}$ mol/cm^3, $D = 5 \times 10^{-19}$ cm^2/s. Values for other parameters are given in Table II.

outlined above provides an enormous advantage over purely empirical methods (*e.g.*, extreme value statistics), in that the distribution function for nucleation and the growth models, and hence the derived damage function, are related to key environmental parameters ($[Cl^-]$, $[O_2]$, pH, T, corrosion potential) analytically. This feature enhances the predictive capabilities of the method and also greatly reduces the amount of data required to "calibrate" the models.

Summary and Conclusions

A review has been presented of the point defect model (PDM) for the growth and breakdown of passive films. While the review necessarily displays the author's bias, the PDM provides a good accounting of the following:

1. The steady-state properties of passive films that form on nickel and tungsten in phosphate buffer solutions at ambient temperature. Diagnostic criteria derived from the PDM demonstrate that the passive film on nickel is a cation conductor whereas that on tungsten is an anion conductor.

2. The electrochemical impedance characteristics of passive nickel in phosphate buffer solution over wide ranges of potential and pH, and at freqencies of the excitation voltage ranging from 10^4 Hz to 10^{-3} Hz, in terms of a single set of kinetic parameters and a potential-dependent parallel capacitance.

Table II. Values for parameters used in calculating damage functions.

Parameter		Value	Units
χ	Passive film stoichiometry	3	
Ω	Mole volume of passive film	30	cm^3/g cation
ΔG°_{A-1}	Gibbs energy of Cl^- absorption	−60	kJ/mol
$\phi^\circ_{f/s}$	Constant, Eq. 17	−0.375	V
ΔG°_s	Gibbs energy of cation vacancy formation	20	kJ/mol
τ	Relaxation time	0	s
ε	Electric field strength	1×10^6	V/cm
T	Temperature	298.15	K
α	Constant, Eq. 17	0.25	
β		−0.001	V
pH		7	
ξ	Critical areal concentration of vacancies	1×10^{16}	No./cm^2
J_m	Vacancy flux in metal phase	0.12×10^7	Vacancies/cm^2 · s
N_o	Surface density of breakdown sites	10^4	No./cm^2
σ_D	Standard deviation in cation vacancy diffusivity	$0.5\bar{D}$	cm^2/s
δh	Pit depth increment	0.05	cm

3. The breakdown of passivity on a wide range of metals and alloys in terms of the formation of cation vacancy condensates.

4. The distributions in the critical breakdown voltage and induction time by assuming that the breakdown sites are distributed with respect to the cation vacancy diffusivity.

5. The role of alloying elements, such as molybdenum, in enhancing the resistance of alloys to passivity breakdown in terms of formation of complexes between the solute (alloying element cation) in the barrier layer and mobile cation vacancies.

6. Transpassive dissolution and electropolishing phenomena, which are attributed to decohesion of the barrier layer due to cation vacancy condensation over macroscopic areas.

7. Erosion-corrosion in which the susceptibility of the barrier layer to shear-induced damage is enhanced by cation vacancy condensation at the metal/film interface.

8. The photoinhibition of passivity breakdown on nickel in terms of photoquenching of the electric field strength.

Additionally, the PDM allows us to formulate a set of principles for designing new alloy systems of superior resistance to passivity breakdown, and to devise new methods for predicting damage functions for localized corrosion. These methods are being used now to predict pitting damage functions for condensing heat exchangers in domestic and industrial gas-fired furnaces and for predicting stress-corrosion-cracking-damage functions for components in the heat-transport circuits of light-water nuclear reactors.

Acknowledgment

The author gratefully acknowledges support of this work by the US Department of Energy/Office of Basic Sciences through Grant No. DE-DG03-84ER45164 and by the Gas Research Institute under Contract No. 5090-260-1969.

Manuscript received March 27, 1992; revised manuscript received July 7, 1992. This was Paper 133 presented at the Phoenix, AZ, Meeting of the Society, Oct. 13-17, 1991.

REFERENCES

1. G. A. Wright, University of Auckland, New Zealand, Private communication (1990).
2. C.-Y. Chao, L.-F. Lin, and D. D. Macdonald, *This Journal*, **128**, 1187 (1981).
3. L.-F. Lin, C.-Y. Chao, and D. D. Macdonald, *ibid.*, **128**, 1194 (1981).
4. C.-Y. Chao, L.-F. Lin, and D. D. Macdonald, *ibid.*, **129**, 1874 (1982).

5. D. D. Macdonald and M. Urquidi-Macdonald, *ibid.*, **137**, 2395 (1990).
6. D. D. Macdonald, S. Biaggio, and H. Song, *ibid.*, **139**, 170 (1991).
7. D. D. Macdonald and S. I. Smedley, *Electrochim. Acta.*, **35**, 1949 (1990).
8. D. D. Macdonald and S. I. Smedley, *Corros. Sci.*, **31**, 667 (1990).
9. D. D. Macdonald and M. Urquidi-Macdonald, *Electrochim. Acta.*, **31**, 1070 (1986).
10. M. Urquidi-Macdonald and D. D. Macdonald, *This Journal*, **134**, 41 (1987).
11. M. Urquidi-Macdonald and D. D. Macdonald, *ibid.*, **136**, 961 (1989).
12. D. D. Macdonald and M. Urquidi, *ibid.*, **132**, 555 (1985).
13. S. Lenhard, M. Urquidi-Macdonald, and D. D. Macdonald, *Electrochim. Acta.*, **32**, 1739 (1987).
14. C. Wagner, *Z. Phys. Chem.*, **B21**, 25 (1933).
15. *Passivity and Its Breakdkown on Iron and Iron-Based Alloys*, R. W. Staehle and H. Okada, Editors, NACE, Houston, TX (1976).
16. *Passivity of Metals and Semiconductors*, M. Fromout, Editor, Elsevier, Amsterdam (1983).
17. *Passivity of Metals*, R. P. Frankenthal and J. Kruger, Editors, The Electrochemical Society, Princeton, NJ (1978).
18. Q. Song, R. C. Newman, R. A. Cottis, and K. Sieradzki, *Corros. Sci.*, **31**, 621 (1990).
19. N. Sato and T. Noda, *Electrochim. Acta.*, **22**, 839 (1977).
20. W. D. Mackintosh and H. H. Plattner, *This Journal*, **124**, 396 (1977).
21. G. B. Naumov, B. N. Ryzhenko, and I. L. Khodakovsky, *Handbook of Themodynamic Data*, English Translation, USGS-WRD-74-001, NTIS, Springfield, VA, (1974).
22. G. C. Wood and J. P. O'Sullivan, *This Journal*, **116**, 1351 (1969).
23. J. R. Park and D. D. Macdonald, *Corros. Sci.*, **23**, 295 (1983).
24. C. B. Bargeron and R. B. Givens, *This Journal*, **124**, 1845 (1977).
25. C. B. Bargeron and R. B. Givens, *Corrosion*, **36**, 618 (1980).
26. J. R. Galvale and S. M. DeMicheli, *Corros. Sci.*, **10**, 795 (1970).
27. Z. A. Foroulis and M. J. Thubrikar, *Electrochim. Acta.*, **21**, 225 (1976).
28. R. S. Alwitt, C. K. Dyer, and B. Noble, *This Journal*, **129**, 711 (1982).
29. D. Ellerbrock and D. D. Macdonald, To be published (1992).
30. T. Koizumi and S. Furuya, *Proc. 2nd Int. Conf. Titanium Sci. Technol.*, **4**, 2383 (1973).
31. T. Shibata, *Trans. ISIJ*, **23**, 785 (1983).
32. T. Shibata and T. Takeyama, *Corrosion*, **33**, 243 (1977).
33. D. D. Macdonald, M. Ben-Hain, and J. Pallix, *This Journal*, **136**, 3269 (1989).
34. E. A. Lizlovs and A. P. Bond, *ibid.*, **122**, 720 (1975).
35. B. A. Shaw, G. D. Davis, T. L. Fritz, B. J. Rees, and W. C. Moshier, *ibid.*, **138**, 3288 (1991).
36. G. D. Davis, W. C. Moshier, G. G. Long, and D. R. Black, *ibid.*, **138**, 3194 (1991).
37. P. M. Natishan, E. McCafferty, and G. K. Hubler, *ibid.*, **133**, 1061 (1986); **135**, 321 (1988).
38. D. H. Bradhurst and J. S. Llewelyn-Leach, *ibid.*, **113**, 1245 (1966).
39. J. S. Llewelyn-Leach and B. R. Pearson, Proc. 7th Int. Congr. Met. Corros., Rio de Janeiro, Brazil, 1978, p. 151.
40. J. S. Llewelyn-Leach, *Proc. Brit. Ceram. Soc.*, **15**, 215 (1970).
41. D. H. Bradhust and J. S. Llewelyn-Leach, *Trans. Brit. Ceram. Soc.*, **62**, 793 (1963).
42. D. A. Vermilyea, *This Journal*, **110**, 345 (1963).
43. H. J. Engell, *Electrochim. Acta*, **22**, 987 (1977).
44. P. A. Jaquet, *Nature*, **135**, 1076 (1935).
45. M. Datta and D. Vercruyssee, *This Journal*, **128**, 1027 (1981).
46. R. Kirchheim, K. Maier, and G. Tölg, *ibid.*, **128**, 1027 (1981).
47. D. D. Macdonald and G. Cragnolino, in *The ASME Handbook on Water Technology for Thermal Power Systems*, P. Cohen and F. J. Pocock, Editors, ASME, New York, (1989).
48. B. C. Syrett, *Corrosion*, **32**, 242 (1976).
49. D. D. Macdonald, B. C. Syrett, and S. S. Wing, *ibid.*, **34**, 289 (1978).
50. D. D. Macdonald, B. C. Syrett, and S. S. Wing, *ibid.*, **35**, 367 (1979).
51. B. C. Syrett, D. D. Macdonald, and S. S. Wing, *Corrosion*, **35**, 409 (1979).
52. D. B. Anderson and F. A. Badia, *J. Eng. Power (Trans. ASME Ser. A)*, **95**, 132 (1973).
53. D. D. Macdonald, C. English, and S. J. Lenhart, Unpublished data (1985).
54. S. J. Lenhart, M. Urquidi-Macdonald, and D. D. Macdonald, *Electrochim. Acta*, **32**, 1739 (1987).
55. Y. Ishikawa, T. Ozaki, N. Hosaka, and O. Nishida, *Trans. ISIG*, **22**, 977 (1982).
56. T. R. Beck and R. C. Alkire, *This Journal*, **126**, 1662 (1979).
57. D. D. Macdonald and M. Urquidi-Macdonald, *Corros. Sci.*, **32**, 51 (1991).